Human brain-derived A oligomers bind to synapses and disrupt synaptic activity in a manner that requires APP

The Journal of Neuroscience

https://jneurosci.msubmit.net

JN-RM-2009-17R1

Human brain-derived Aβ oligomers bind to synapses and disrupt synaptic activity in a manner that requires APP

Dominic Walsh, Harvard Institutes of Medicine
Zemin Wang, Brigham and Women's Hospital and Harvard Medical School
Rosemary Jackson, University of Edinburgh
Wei Hong, Brigham and Women's Hospital and Harvard Medical School
Walter Taylor, Brigham and Women's Hospital and Harvard Medical School
Grant Corbett, Brigham and Women's Hospital, Harvard Medical School
Arturo Moreno, UCSF
Wen Liu, Brigham and Women's Hospital and Harvard Medical School
Shaomin Li, Brigham and Women's Hospital and Harvard Medical School
Matthew Frosch, Massachusetts General Hospital
Tracy Young-Pearse, Brigham and Women's Hospital, Harvard Medical School and Ann Romney Center for Neurologic Diseases
Inna Slutsky, Tel Aviv University
Tara Spires-Jones, University of Edinburgh

Commercial Interest:

Human brain-derived Aβ oligomers bind to synapses and disrupt synaptic activity in a manner that requires APP

Zemin Wang[1], Rosemary J. Jackson[2], Wei Hong[1], Walter M. Taylor[1], Grant T. Corbett[1], Arturo Moreno[1], Wen Liu[1], Shaomin Li[1], Matthew P. Frosch[3], Inna Slutsky[4], Tracy Young-Pearse[1], Tara L. Spires-Jones[2], and Dominic M. Walsh[1]*

[1]Laboratory for Neurodegenerative Research, Ann Romney Center for Neurologic Diseases, Brigham and Women's Hospital and Harvard Medical School, Boston, MA 02115, USA; [2]The University of Edinburgh, UK Dementia Research Institute, 1 George Square, Edinburgh, UK; [3]Massachusetts General Institute for Neurodegenerative Disease, Massachusetts General Hospital and Harvard Medical School, Charlestown, MA 02129, USA; and [4]Department of Physiology and Pharmacology, Sackler Faculty of Medicine, Tel Aviv University; 69978 Tel Aviv, Israel.

*Correspondence to dwalsh3@bwh.harvard.edu

Running title: Aβ-mediated disruption of synaptic activity requires APP.

Number of Pages: 63
Number of Figures: 11
Number of Tables: 1
Number of words for Abstract: 161
Number of words for Introduction: 652
Number of words for Discussion: 1387

Acknowledgments

We thank Dr. Tiernan T. O'Malley for useful discussions and technical advice. This work was supported by grants to DMW from the National Institutes of Health (AG046275), Bright Focus, and the United States-Israel Binational Science Foundation (2013244, DMW and IS); grants to TSJ from Alzheimer's Research UK and the Scottish Government (ARUK-SPG2013-1), Wellcome Trust-University of Edinburgh Institutional Strategic Support funds, and the H2020 European Research Council (ALZSYN); and to the Massachusetts Alzheimer's Disease Research Center (AG05134). TSJ is a member of the FENS Kavli Network of Excellence.

Abstract

Compelling genetic evidence links the amyloid precursor protein (APP) to Alzheimer's disease (AD), and several theories have been advanced to explain the involvement of APP in AD. A leading hypothesis proposes that a small amphipathic fragment of APP, the amyloid β-protein (Aβ), self-associates to form soluble aggregates which impair synaptic and network activity. Here, we employed the most disease-relevant form of Aβ, protein isolated from AD brain. Using this material, we show that the synaptotoxic effects of Aβ depend on expression of APP and that the Aβ-mediated impairment of synaptic plasticity is accompanied by pre-synaptic effects which disrupt the excitatory/inhibitory (E/I) balance. The net increase in the E/I ratio, and inhibition of plasticity are associated with Aβ localizing to synapses and binding of soluble Aβ aggregates to synapses requires the expression of APP. Taken together, our findings indicate a role for APP in AD pathogenesis beyond the generation of Aβ and suggest modulation of APP expression as a therapy for AD.

Significance Statement

Here, we report on the plasticity-disrupting effects of Aβ isolated from AD brain and the requirement of APP for these effects. We show that Aβ-containing AD brain extracts block hippocampal long-term potentiation (LTP), augment glutamate release probability and disrupt the excitation/inhibition balance. Notably, these effects are associated with Aβ localizing to synapses, and genetic ablation of APP prevents both Aβ binding and Aβ-mediated synaptic dysfunctions. Our results emphasize the importance of APP in AD and should stimulate new studies to elucidate APP-related targets suitable for pharmacological manipulation.

Introduction

Mutation, over-expression or altered processing of the amyloid precursor protein (APP) underlie all known monogenic cases of familial Alzheimer's disease (fAD) (Tanzi, 2012; Guerreiro and Hardy, 2014). Although the physiological roles of APP are not fully understood, a myriad of studies indicate that APP plays a role in synaptic plasticity, dendritic morphogenesis, and neuroprotection (Muller and Zheng, 2012). Membrane-tethered APP can act as a cell-adhesion molecule linking the pre-and post-synapse (Soba et al., 2005) and APP has been shown to regulate synaptic vesicle proteins, synaptic transmission and plasticity (Dawson et al., 1999; Lassek et al., 2013; Fanutza et al., 2015; Lassek et al., 2016). In the rat dentate gyrus (DG), APP expression is known to change during memory consolidation (Conboy et al., 2005) and intraventricular administration of anti-APP antibodies or antisense oligonucleotides results in profound amnesia (Doyle et al., 1990; Huber et al., 1993; Mileusnic et al., 2000). Notably, APP is a component of the presynaptic GABA-B1a receptor ($GABA_{B1a}$-R) complex (Bai et al., 2008; Schwenk et al., 2016) and neuron-type specific knock-out of APP indicates an important role for APP in GABAergic transmission and maintenance of the excitatory–inhibitory balance (Wang et al., 2014).

APP is a complex molecule that undergoes substantial post-translational modification and processing as more than 10 different proteolytic fragments of APP have been identified. Several of these are suggested to be pathogenic (Neve and McPhie, 2007; Yankner and Lu, 2009; Tamayev et al., 2012; Welzel et al., 2014; Willem et al., 2015), whereas others are neuroprotective (Mockett et al., 2017). The fragment from which the

precursor protein derives its name, the amyloid β-protein (Aβ), is found in the tell-tale amyloid plaques which populate brains of individuals who die with AD. Aβ comprises a family of APP-derived peptides that share a common core of ~30 amino acids (Walsh and Teplow, 2012) which are produced by the concerted action of two aspartyl proteases, β–secretase and γ-secretase (De Strooper, 2010). Aβ peptides are prone to self-associate and multiple studies indicate that certain forms of Aβ adversely affect synaptic form and function (Li et al., 2009).

The synaptotoxic activity of Aβ and the involvement of APP in synapse formation and activity are particularly relevant to AD since *in vivo* and postmortem studies indicate that synapse dysfunction and loss are prominent early features of AD (Scheff et al., 2006; Scheff et al., 2007; Johnson et al., 2012). Acute studies in wild-type rodents show that non-fibrillar, water-soluble Aβ from a variety of sources are potent synaptotoxins (Lambert et al., 1998; Walsh et al., 2002; Cleary et al., 2005; Lesne et al., 2006; Klyubin et al., 2008; Minkeviciene et al., 2009; Kurudenkandy et al., 2014). Furthermore, *in vitro* and *in vivo* studies demonstrate that the most disease-relevant form of non-fibrillar Aβ, Aβ extracted from the water-soluble phase of AD brain, inhibits long-term potentiation (LTP), facilitates long-term depression (LTD), reduces synaptic remodeling, and impairs memory consolidation (Shankar et al., 2008; Barry et al., 2011; Freir et al., 2011; Borlikova et al., 2013; Jo et al., 2014; Yang et al., 2017). Here, we show that the block of LTP mediated by Aβ-containing AD brain extracts is accompanied by opposing changes in excitatory and inhibitory pre-synaptic release probabilities and consequent disruption of the excitation/inhibition (E/I) balance. The net increase in the E/I ratio and inhibition of LTP require expression of APP and are associated with Aβ localizing to

synapses. These findings suggest a link between Aβ toxicity and perturbation of the normal regulatory role of APP, and are consistent with prior studies which have imputed a role for APP in Aβ toxicity (White et al., 1998; Lorenzo et al., 2000; Shaked et al., 2006; Sola Vigo et al., 2009; Fogel et al., 2014; Kirouac et al., 2017). In light of these results we suggest that down-regulation of APP expression or modulation of its interaction with synaptotoxic Aβ species should be investigated as an approach to treat AD.

Materials and Methods

Reagents

All chemicals and reagents were purchased from Sigma-Aldrich unless otherwise noted. Synthetic Aβ1–42 was synthesized and purified using reverse-phase HPLC by Dr. James I. Elliott at the ERI Amyloid laboratory (Oxford, CT, USA). Peptide mass and purity (>99%) were confirmed by reverse-phase HPLC and electrospray/ion trap mass spectrometry. N-terminally extended (NTE) -31Aβ-40 was prepared and purified as described previously (Mc Donald et al., 2015) and recombinant Aeta-alpha (Aη−α, $APP_{505-611}$) was a gift from Drs. Willem and Haass (Ludwig-Maximillian University, Munich).

Antibodies

The antibodies used and their source are described in Table 1.

Preparation of human brain extracts

All human specimens were obtained and used in accordance with the Partner's Institutional Review Board (Protocol: Walsh BWH 2011). Brain tissue was obtained from 2 of individuals (referred to as AD1 and AD2) who died with AD and one individual who died free of AD (designated NC). AD1 was an 87-year-old man who 9 months prior to death had scored 23 on the MMSE and designated Braak stage 4 at postmortem had

pathological changes consistent with mild AD. AD2 was a 68-year-old female with end-stage AD. Three years prior to death AD2 scored 23 on the MMSE, but in her last weeks she was unable to answer questions other than to provide her first name. Upon postmortem examination there was evidence of fulminant amyloid and neurofibrillary tangle pathology which was designated Braak stage V/VI. Neither AD1 nor AD2 had a family history of AD. NC was a 58-year-old female who died free of AD symptoms and pathology. AD1 and NC has post-mortem intervals (PMI) of 18 hours, and AD had a PMI of 12 hours. Aqueous extracts of brain were prepared by homogenizing cortical tissue in a buffer which we refer to as artificial cerebrospinal fluid base buffer (aCSF-B) (124 mM NaCl, 2.8 mM KCl, 1.25 mM NaH_2PO_4, 26 mM $NaHCO_3$, pH 7.4). aCSF-B is the core buffer used in subsequent electrophysiology experiments. Whole frozen temporal cortex was left at 4^{o}C until the tissue was sufficiently soft to cut. Meninges and large blood vessels were removed and gray matter dissected from white matter. The total amount of gray matter obtained was between 12-14 g. Two gram lots of tissue were diced using a razor blade and then homogenized in 10 ml of ice-cold aCSF-B (containing 5 mM Ethylenediaminetetraacetic acid, 1 mM Ethyleneglycoltetraacetic acid, 5 µg/ml Leupeptin, 5 µg/ml Aprotinin, 2 µg/ml Pepstatin, 120 µg/ml Pefabloc and 5 mM NaF) with 25 strokes of a Dounce homogenizer (Fisher, Ottawa, Canada). Homogenates from 6, 2 g lots were pooled and centrifuged at 198,000 *g* and 4°C for 110 minutes in a SW 41-Ti rotor (Beckman Coulter, Fullerton, CA). The upper 90% of supernatant was dialyzed (using Slide-A-Lyzer™ G2 Dialysis Cassettes, 2K MWCO, Fisher Scientific) against fresh aCSF-B to remove bioactive small molecules and drugs. Dialysis was performed at 4^{o}C against a 100-fold excess of buffer with buffer changed 3

158 times over a 36 hour period. Thereafter, extracts were divided into 2 parts: 1 portion
159 was immunodepleted (ID) of Aβ by 3 rounds of 12 hour incubations with the anti-Aβ
160 antibody, AW7, plus Protein A sepharose (PAS) beads at 4 ^{o}C (Freir et al., 2011). The
161 second portion was treated in an identical manner, but this time incubated with pre-
162 immune serum plus PAS beads. Samples were cleared of beads and 0.5 ml aliquots
163 stored at -80^{o}C until used for biochemical or electrophysiological experiments. Samples
164 were thawed only once prior to use.
165
166 **Preparation of amyloid-derived diffusible ligands (ADDLs)**
167 Amyloid-derived diffusible ligands (ADDLs) were prepared essentially as described
168 previously (Freir et al., 2011). Hexafluoro-2-propanol (HFIP; 222 μl) was added to 1 mg
169 of Aβ(1–42) in a 2 ml low-binding microcentrifuge tube to produce a peptide
170 concentration of 1 mM. The solution was split into two tubes, incubated at 37°C for 1
171 hour and mixed by vortexing every 10 minutes. The HFIP was gently evaporated under
172 a nitrogen stream with rotation of the tube to ensure formation of an even film of peptide
173 on the lower walls of the tube. Dried peptide films were stored over desiccant at 20°C
174 for a minimum of 14 hours. The peptide film from each tube was then dissolved in 20 μl
175 of anhydrous DMSO (Life Technologies, Woburn, MA) and 5 μl lots of the DMSO
176 mixture was added stepwise to 980 μl of F-12 medium (Life Technologies), with
177 vortexing between each addition. The resulting solution was incubated at 4°C for 48
178 hours and then centrifuged at 16,000 *g* for 10 minutes. The upper 95% of the
179 supernatant was transferred to a new microcentrifuge tube and the protein

concentration determined using the extinction coefficient, ε_{275} = 1361 M^{-1} cm^{-1} (O'Malley et al., 2014). Aliquots were then immediately frozen on dry ice and stored at -80°C.

Characterization of ADDLs

The size and morphology of structures present in the ADDLs preparation were investigated using negative contrast electron microscopy and analytical size exclusion chromatography (SEC). Samples were stained and visualized essentially as described previously (Betts et al., 2008). An aliquot of the ADDL preparation (50 µl) was diluted 1:1 with F12 media and then adsorbed (10 µl) onto formvar-coated copper grids (Electron Microscopy Sciences). After 1 minute, 10 µl 0.25% glutaraldehyde was added and incubated for 1 minute. Thereafter, grids were wicked dry using filter paper, washed twice with MilliQ water and then stained with 1% uranyl-acetate for 2 minutes. Grids were allowed to air dry for at least 10 minutes, stored at room temperature and then examined using a 1200EX microscope (JEOL).

A separate aliquot of ADDLs (50 µl) was thawed and loaded on to a Superdex 75 3.2/300 PE column (GE Healthcare) eluted in PBS pH 7.4 at 0.8 ml/min using a Shimadzu HPLC system.

Preparation of synthetic peptides used for Western blotting

Aηα peptide was dissolved in 50 mM ammonium bicarbonate, pH 8.5, diluted to 10 ng/µl, aliquoted and stored frozen at -80°C. Aβ1-42 and -31Aβ40 which are prone to aggregate were treated to depolymerize any pre-existing aggregates. Briefly, peptides were dissolved in 50 mM Tris-HCl, pH 8.5, containing 7 M guanidium-HCl (GuHCl) and

5 mM ethylenediaminetetraacetic acid (EDTA) at a concentration of 1 mg/ml and incubated at room temperature (RT) overnight. Samples were then centrifuged for 30 minutes at 16,000 *g* and chromatographed on a Superdex 75 10/300 column eluted at 0.5 ml/min with 50 mM ammonium bicarbonate, pH 8.5. The concentration of the peak fraction for each sample was determined by absorbance at 275 nm. The peptide was then diluted to 10 ng/µl, aliquoted and stored frozen at -80°C.

Immunoprecipitation/Western blotting (IP/WB) of Aβ in brain extracts

Extracts were first pre-cleared with PAS beads to minimize non-specific interactions in the subsequent IP. One ml aliquots of extracts were incubated with 15 µl PAS beads for 1 hour at 4°C with gentle shaking. PAS beads were removed by centrifugation (4000 *g* for 5 minutes) and the supernatant divided into 0.5 ml aliquots. Each aliquot was incubated with 10 µl of AW7 and 15 µl PAS beads overnight at 4°C with gentle shaking. Aβ-antibody-PAS complexes were collected by centrifugation and washed as previously described (Shankar et al., 2011). The immunoprecipitated (IP'd) Aβ was eluted by boiling in 18 µl of 1 × sample buffer (50 mM Tris, 2% w/v SDS, 12% v/v glycerol with 0.01% phenol red) and electrophoresed on hand poured, 15 well 16% polyacrylamide tris-tricine gels. Aη–α, Aβ1-42 and -31Aβ40 were run as loading controls and protein transferred onto 0.2 µM nitrocellulose at 400 mA and 4^{o}C for 2 hour. Blots were microwaved in PBS and Aβ detected using the anti-Aβ40 and anti-Aβ42 antibodies, 2G3 and 21F12, and bands visualized using a Li-COR Odyssey infrared imaging system (Li-COR, Lincoln, NE). To determine if AW7 IP'd other APP

metabolites (e.g. APPsα, N-terminally extended Aβ or Aη peptides) from AD brain extracts, certain blots were developed with 6E10 (Table 1).

MSD Aβ immunoassays

Samples were analyzed for Aβ content using 2 distinct assay formats: the Aβx-42 assay that preferentially detects Aβ42 monomers and the oAssay that preferentially detects Aβ oligomers and aggregates (Mably et al., 2015; Yang et al., 2015). Immunoassays were performed using the Meso Scale Discovery (MSD) platform and reagents from Meso Scale (Rockville, MD). The Aβx-42 assay uses mAb m266 (3 µg/ml) for capture and biotinylated 21F12 (1 µg/ml) for detection, and the oAssay uses mAb 1C22 (3 µg/ml) for capture and biotinylated 3D6 (1 µg/ml) for detection. Samples, standards and blanks were loaded in duplicate and analyzed as described previously (Mably et al., 2015).

Since Guanidine Hydrochloride (GuHCl) effectively disaggregates high molecular weight Aβ species (Mably et al., 2015), samples were analyzed both with and without incubation in 5 M GuHCl. Analysis of samples in the absence of GuHCl allows the measurement of native Aβ42 monomer using the Aβx-42 assay, and native Aβ aggregates using the oAssay. Analysis of samples treated with GuHCl allows detection of disassembled aggregates with Aβx-42 assay. To dissociate aggregates, 20 µl of extract was incubated overnight with 50 µl of 7 M GuHCl at 4°C. Thereafter samples were diluted 1:10 with assay diluents so that the final GuHCl concentration was 0.5 M. Aβ standards were prepared in tris-buffered saline (TBS), pH 7.4 containing 0.5 M

GuHCl, 0.05% Tween 20 and 1% Blocker A so that both standards and samples contained the same final concentration of GuHCl.

Mice

All animal procedures were performed in accordance with the National Institutes of Health Policy on the Use of Animals in Research and were approved by the Harvard Medical School Standing Committee on Animals. Wild-type (WT) C57BL/6 mice were purchased from the Jackson Laboratory (Bar Harbor, ME). APP KO mice on a C57BL/6 background and littermate WT controls were obtained from the Young-Pearse lab (Callahan et al., 2017). A second line of APP KO mice were purchased from the Jackson Laboratory (APP^{tm1Dbo}/J, The Jackson Laboratory, Bar Harbor, ME) (Zheng et al., 1995) and for certain experiments these animals were bred with WT C57BL/6 mice to generate APP (+/-) hemizygotes. Animals were housed in a room with a 12 hour light/dark circadian cycle with *ad libitum* access to food and water. Mice were genotyped by PCR prior to use, and both male and female mice were used. In certain experiments, upon completion of electrophysiological recordings, brain slices were used for Western blotting or array tomography.

Brain slice preparation

Two to three months old male and female animals were anaesthetized with isoflurane and decapitated. Brains were rapidly removed and immediately immersed in ice-cold

(0-4°C) artificial cerebrospinal fluid (aCSF). The aCSF contained (in mM): 124 NaCl, 3 KCl, 2.4 $CaCl_2$, 2 $MgSO_4 \cdot 7H_2O$, 1.25 NaH_2PO_4, 26 $NaHCO_3$ and 10 D-glucose, and was equilibrated with 95% O_2 and 5% CO_2, pH 7.4, 310 mOsm. Coronal brain slices (350 μm), including hippocampus (Wang et al., 2008), were prepared using a Leica VT1000 S vibratome (Leica Biosystems Inc, Buffalo Grove, IL), transferred to an interface chamber and incubated at 34 ± 5°C for 20 minutes and then kept at room temperature for 1 hour before recording.

Long-term potentiation (LTP) recording

Brain slices were transferred to a submerged recording chamber and perfused (10 ml/min) with oxygenated (95% O_2 and 5% CO_2) aCSF 10 minutes before electrophysiological recordings. Brian slices were visualized using an infrared and differential interference contrast camera (IR-DIC camera, Hitachi, Japan) mounted on an upright Olympus microscope (Olympus, Tokyo, Japan). Recording electrodes were pulled from borosilicate glass capillaries (Sutter Instruments, Novato, CA) using a micropipette puller (Model P-97; Sutter Instruments, Novato, CA) with resistance ~2 MΩ when filled with aCSF. To induce field excitatory post-synaptic potentials (fEPSPs) in the hippocampal CA1, a tungsten wire stimulating electrode (FHC, Inc., Bowdoin, ME) was placed on the Schaffer collaterals of the CA3 and a recording electrode was placed at least 300 μm away on the striatum radiatum of the CA1. The initial 10-40 % slope of fEPSPs were calculated. Test stimuli were delivered once every 20 seconds (0.05 Hz) and the stimulus intensity was adjusted to produce a baseline fEPSP of 30–40% of the maximal response. A stable baseline was recorded for at least 10 minutes prior to

addition of sample. Thirty minutes following application of sample, LTP was induced by theta burst stimulation (TBS). This involved 3 trains, each of 4 pulses delivered at 100 Hz, 10 times, with an interburst interval of 200 milli-second with a 20 second interval between each train. Field potentials were recorded using a Multiclamp amplifier (Multiclamp 700B; Molecular Devices, Sunnyvale, CA) coupled to a Digidata 1440A digitizer. Signal was sampled at 10 kHz and filtered at 2 kHz and data were analyzed using Clampex 10 software (Molecular Devices, Sunnyvale, CA).

Whole-cell patch clamp recording

Brain slices were prepared from male and female WT and APP KO mice (1-2 months old) as described above for LTP experiments but using a cutting solution that contained sucrose (in mM: 72 sucrose, 83 NaCl, 2.5 KCl, 1 NaH_2PO_4, 3.3 MgSO4·7H2O, 26.2 $NaHCO_3$, 22 dextrose, and 0.5 $CaCl_2$) saturated with 95% O_2 and 5% CO_2, pH 7.4, 310 mOsm (Wang et al., 2015). Slices were incubated in oxygenated slicing solution for 20 minute, and held at room temperature for a further 40 minute prior to recording. Slices were transferred to a submerged recording chamber and perfused (10 ml/min) with oxygenated (95% O_2 and 5% CO_2) aCSF for 30 minute at room temperature. Whole-cell recordings were made from the somata of CA1 pyramidal neurons visualized using an IR-DIC camera mounted on an upright Olympus microscope (Olympus, Tokyo, Japan). Patch pipettes (4–7MΩ) were filled with an internal solution containing (in mM): 120 CsGluconate, 5 $MgCl_2$, 0.6 EGTA, 30 HEPES, 4 MgATP, 0.4 Na_2GTP, 10 phosphocreatine-Tris, 5 N-(2,6-Dimethylphenylcarbamoylmethyl)triethylammonium bromide (QX-314); 290 mOsm; pH was adjusted to 7.2 with CsOH. Signal was

acquired using a Multiclamp amplifier (Multiclamp 700B; Molecular Devices, Sunnyvale, CA) with Clampex 10 software (Molecular Devices, Sunnyvale, CA), sampled at 10 kHz and filtered at 2 kHz. Data were stored on a PC after digitization by an A/D converter (Digidata 1440A, Molecular Devices, Sunnyvale, CA) for offline analysis. Membrane potential was corrected for the liquid junction potential of 13.7 mV. Neurons with negative resting membrane potential less than -60 mV were not analyzed. Input resistance and patching access resistance were continuously monitored during the experiment and cells which exhibited more than 15–20% changes in these parameters were excluded from analysis.

In order to preserve a relatively intact neuronal circuit, no receptor antagonists were used. Spontaneous excitatory post-synaptic currents (sEPSCs) were collected at a membrane holding potential of -70 mV, which is close to the calculated reverse potential of GABA. In order to measure the excitatory and inhibitory input on the same neuron, the spontaneous inhibitory post-synaptic currents (sIPSCs) were also measured on the same neuron but this time the holding potential was increased to 5-10 mV, a potential close to the reverse potential of excitatory input, without visual negative deflection. Recorded neuronal activities were detected as described previously (Lillis et al., 2015) by custom software (DClamp: available at www.ieeg.org/?q=node/34). Integrated excitatory conductance (sEPSCs, G_E) and integrated inhibitory conductance (sIPSCs, G_I) were calculated as previously reported $G_E = \int_0^t \frac{sEPSCs}{t(V_M - V_{Erev})}$ and $G_I = \int_0^t \frac{sIPSCs}{t(V_M - V_{Irev})}$ (Slomowitz et al., 2015).

Preparation of mouse brain homogenates and detection of APP

Certain brain slices from wild-type and APP knock-out mice were frozen immediately after completion of electrophysiological recording (Figures 4, 5 and 6) and stored at -80^{o}C until analyzed. Tissue (~0.1 mg) was homogenized in 5 volumes (w/v) of ice-cold 20 mM Tris-HCl, containing 150 mM NaCl and 1%TX-100 (TBS-Tx), pH 7.4 containing protease inhibitors and centrifuged at 100,000 *g* and 4°C for 78 minutes in a TLA-55 rotor (Beckman Coulter, Fullerton, CA). The upper 90% of the supernatant was removed, aliquoted and stored at -80°C pending analysis. Ten µg of total protein was boiled in 1 × sample buffer (62.5 mM Tris, 1% w/v SDS, 10% v/v glycerol, 0.01% phenol red and 2% β-mercaptoethanol) for 5 minutes and electrophoresed on hand poured, 15 well 10% polyacrylamide tris-glycine gels. Gels were rinsed in transfer buffer (10% methanol, 192 mM Glycine and 25 mM Tris) and proteins electroblotted onto 0.2 µM nitrocellulose membranes at 400 mA and 4°C for 2.5 hours. Membranes were developed using the anti-APP antibody, 22C11, and bands visualized using a Li-COR Odyssey infrared imaging system (Li-COR, Lincoln, NE).

Array tomography (AT) imaging of mouse brain slices

Upon completion of electrophysiology recordings certain brain slices from wild-type and APP knock mice (Figures 4, 5 and 6) were processed for array tomography (Koffie et al., 2009; Pickett et al., 2016). Slices were fixed in PBS containing 4% paraformaldehyde and 2.5% sucrose at 4°C overnight. Samples were then washed three times (10

minutes each) in cold wash buffer (PBS containing 3.5% sucrose and 50 mM glycine), and the hippocampus dissected out under a Leica Wild M3Z Stereozoom Microscope (Heerbrugg, Swizerland). Thereafter hippocampi were dehydrated using an ethanol gradient of: 50%, 70%, 95% and 100%. Tissue was then placed into a solution of 1:1 ethanol: LR White resin (Electron Microscopy Sciences) for 5minute and then washed 3 times with LR White. Tissue was incubated overnight at 4°C in LR White, embedded in a gelatin capsule and polymerized overnight at 53°C. Three embedded blocks per condition were cut into ribbons of 70 nm sections on an ultracut microtome (Leica) using a Jumbo Histo Diamond Knife (Diatome). Ribbons were collected on gelatin-coated glass coverslips, stained with antibodies and imaged along the ribbon. Two ribbons per slice were collected and one was stained for PSD95 and 1C22 and the other for synapsin-1 and 1C22. Primary antibodies were 1C22 (1:50), rabbit anti-PSD95 (3450P, Cell Signaling, at 1:50), and rabbit anti-synapsin-1 (AB1543P, Millipore, at 1:100). Secondary antibodies donkey anti-mouse 488 (A21202) and donkey anti-rabbit 594 (A21207) were from Invitrogen and used at 1:50.

Two image stacks per ribbon were collected from the stratum radiatum using a Zeiss axio Imager Z2 epifluorescent microscope with a 63X 1.4NA Plan Apochromat objective. Images were acquired with a CoolSnap digital camera and AxioImager software with array tomography macros (Carl Zeiss, Ltd, Cambridge UK). Images from each set of serial sections were compiled to create a 3D stack and aligned using ImageJ multistackreg macros (Kay et al., 2013). Regions of interest (10 μm x 10 μm) were selected, cropped and thresholded in Image J (Schindelin et al., 2012; Ollion et al., 2013) (Figure 1). Custom MATLAB macros were used to remove single slice punctuate,

count synaptic punctuate and assess co-localization with 1C22 (a minimum of 50% overlap between 1C22 and synaptic punctuate was required to be designated as co-localization). All custom analysis macros will be freely available on http://datashare.is.ed.ac.uk after publication.

Data analysis and Statistical test

Figures showing IP/WB and MSD Aβ immunoassay data are representative of at least 2 independent experiments. For electrophysiological experiments, the AD, ID-AD and aCSF samples were coded and tested in an interleaved manner to avoid variances in animals or slice quality influencing results. Slices in each group came from different animals unless otherwise noted. Electrophysiological data were analyzed offline by pclamp 10.2 (Molecular Devices, Sunnyvale, CA) and tested with One-way or Two-way analysis of variance (ANOVA) with Bonferroni *post-hoc* tests or student's *t*-tests (# $p<0.05$, ## $p< 0.01$, and ### $p< 0.001$). A Kolmogorov–Smirnov (K–S) test was used to compute differences in distributions of sEPSCs and sIPSCs. Array tomography was analyzed using SPSS Version 22. A single percent co-localization for each parameter was calculated for each slice from approximately 41 regions of interest and ≈7,500 synapses (~3,500 pre-synapses and ~3,500 post-synapses) were analyzed per slice and tested with a Kruskal-Wallis with Dunns *post-hoc* test. Electrophysiology data are shown as means ± SEM. Array tomography data is shown as medians ± the interquartile range, each point representing all synapses measured within 1 slice.

Analyses of the same sample using different slices are considered technical replicates and analysis of extracts from different AD brains are considered biological replicates.

Results

We previously reported that aqueous extracts of certain end-stage AD brains block hippocampal LTP *in vivo* and *in vitro* (Shankar et al., 2008; Barry et al., 2011; Freir et al., 2011; Jo et al., 2014). Here we further investigated the mechanism of this effect and the requirement of endogenous APP.

The water-soluble extract from AD brain contains both Aβ monomers and oligomers and blocks LTP in a manner dependent on Aβ

Brain extracts were prepared as described and a portion was immunodepleted (ID) of Aβ or mock-ID with pre-immune rabbit serum. Here, the mock-ID extract is referred to as the AD sample, and the material depleted of Aβ as ID-AD. ID and AD samples from AD1 were analyzed using IP/WB, and MSD immunoassays that preferentially recognize either Aβ oligomers (oAssay) or Aβ42 monomers (Mc Donald et al., 2015). IP/WB analysis allows the capture of Aβ structures under native conditions and their detection following denaturing SDS-PAGE. We were careful to also determine if AW7 altered APP metabolites present in AD brain extracts that contained all or part of the Aβ sequence i.e. APPsα, N-terminally extended Aβ (-31Aβ40), or so-called Aη peptides. To this end AW7 IPs were used for Western blotting with (i) the C-terminal anti-Aβ antibodies, 2G3 and 21F12, and (ii) the N-terminal anti-Aβ antibody, 6E10. The latter, but not the former, reacts with APPsα and Aη–α peptides (Portelius et al., 2013; Welzel et al., 2014; Willem et al., 2015). 6E10 readily detected ~4 kDa Aβ, but it did not detect

any bands consistent with APPsα or Aη−α. Furthermore, direct Western blot analysis of AD brain extract demonstrated highly similar levels of APPs in both AW7 and mock immunodepleted extracts. Thus, it appears that AW7 does not deplete AD extracts of non-Aβ APP metabolites that contain the N-terminal portion of Aβ (Figure 2A). The ~7 kDa Aβ species detected with 2G3 and 21F12 was not detected with 6E10, consistent with our prior observation that most ~7 kDa Aβ is N-terminally truncated - a pattern we have seen in aqueous extracts of more than 100 AD brains analyzed in our laboratory (Mc Donald et al., 2015). Since SDS-PAGE is highly denaturing, the ~4 and ~7 kDa species do not necessarily reflect native Aβ species. Rather, these simply indicate that at least two different Aβ species are present. The same samples were treated with or without 5 M GuHCl and then analyzed using MSD assays. In prior studies we found that GuHCl effectively disaggregates high molecular weight Aβ species such that the signal detected by our oAssay is greatly decreased, whereas the signal detected by the monomer-preferring Aβx-42 immunoassay is proportionately increased (Mably et al., 2015). A similar outcome was evident when the extract of AD1 was treated with GuHCl (Figure 2B). Specifically, GuHCl treatment caused a ~70% decrease in the oligomer signal and a more than 8-fold increase in the monomer signal. Together these immunoassay and IP/WB results indicate that the majority of Aβ in the AD1 extract exist as labile aggregates made up of ~4 kDa Aβ and ~7 kDa Aβ. Importantly, AW7 ID effectively removed the large majority of the various Aβ species detected (Figure 2A and B). For instance, AW7 ID reduced the oligomer signal from 5.1 ± 0.03 ng/ml to 0.32 ± 0.12 ng/ml (Figure 2B, left panel) and monomer from 3.42 ± 0.03 ng/ml to 0.12 ± 0.04 ng/ml (Figure 2B, right panel).

For slices that received vehicle aCSF-B (Control), TBS induced strong potentiation which lasted the whole recording period (Figure 2C, black circles, 181.1 ± 10.7 %, *n* = 17), and ID-AD1 allowed a similar response (green downward triangles, 173.6 ± 8.7 %, *n* = 11, *p*=0.12, One-Way ANOVA) (Figure 2C and D). Consistent with prior reports (Shankar et al., 2008; Freir et al., 2011), application of the AD1 (magenta diamonds) extract significantly decreased LTP compared to both the control and ID-AD1 treatment (136 ± 4.2 %, *n* = 18, F=4.26，*p*=6.98E-9 AD1 vs. Control; F=4.14, *p*=3.56E-12 AD1 vs. ID-AD1, One-Way ANOVA). The fact that the ID-AD1 and AD1 samples are identical except that the latter contains more Aβ than the former, is evidence that some form of Aβ is responsible for the block of LTP induced by the AD1 extract. To further test the Aβ dependency of the block of LTP mediated by AD1, we examined whether an extract from a non-AD brain (NC), could impair LTP. As anticipated, the NC extract lacked appreciable levels of Aβ (not shown) and did not impair LTP (Figure 2E and F, 159.54 ± 10.6 % in NC, *n* = 8; 160.36 ± 6.26 % in Control, *n* = 8; F=4.6，*p*=0.95 One-Way ANOVA).

Aβ-containing AD brain extract affects pre-synaptic release probabilities

Accumulating evidence indicates that soluble Aβ species may interact with excitatory and inhibitory pre-synaptic terminals, modulate neurotransmitter release and cause synaptic dysfunction in the very early stages of AD (Nimmrich et al., 2008; Abramov et al., 2009; Kabogo et al., 2010; Parodi et al., 2010; Russell et al., 2012; Sokolow et al., 2012; Huang et al., 2013; Ripoli et al., 2013; Kurudenkandy et al., 2014). Although the

effects of Aβ on LTP are well established (Klyubin et al., 2012), little is known about whether and how Aβ-containing AD extracts affect pre- and post-synaptic elements. To investigate effects on pre-synaptic release, we measured short-term synaptic facilitation (Zucker and Regehr, 2002) in slices before and 30 minutes after treatment with AD1 extract. As synapse release probability is inversely correlated to synaptic facilitation (Zucker and Regehr, 2002), we employed high-frequency burst stimulation (5 pulses with 20 millisecond intra-burst stimulus interval). Application of AD1 extract induced a reduction in the short-term facilitation during burst stimulation (Figure 3A and B). When responses were normalized based on the ratio of each fEPSP to the first response, we found that treatment with AD1 extract had no effect on the 2^{nd} response, but significantly decreased the 3^{rd}, 4^{th}, and 5^{th} response (magenta circles, p=0.02 at 3^{rd} stimulation, p=0.004 at 4^{th} stimulation and p=0.004 at 5^{th} stimulation, n = 6, student's t-test, and also by group and time with Two-way ANOVA, $F_{(4,7)}$=6.39, p=0.006) (Figure 3B). In contrast, the slices treated with ID-AD1 yielded a pattern highly similar to that obtained with aCSF-B control (n = 7, F=5.32, p=0.91, Two-Way ANOVA, Figure 3C and D). Thus, Aβ in the AD extract caused a reduction in short-term synaptic plasticity associated with increased pre-synaptic glutamate release.

Aβ-containing AD brain extract disrupts the excitation-to-inhibition balance

To estimate the effect of Aβ on the total synaptic input at the single-neuron level, we used whole-cell voltage clamp recordings to measure spontaneous excitatory postsynaptic currents (sEPSCs) on CA1 pyramidal neurons before and 30 minutes after

addition of AD extract. The holding potential was kept constant at -70 mV and sEPSCs measured before and 30 minutes after addition of AD1 extract – this 30 minutes interval was chosen to match the pre-incubation time used in our LTP and short-term facilitation experiments. Application of the AD1 extract significantly decreased the inter-event interval (p=1.65E-6, K-S test) and increased the mean frequency of sEPSCs (from 1.8 ± 0.2 Hz to 2.7 ± 0.3 Hz, p=0.02, n = 7, student's t-test) (Figure 4A and B), but did not alter the sEPSCs amplitude (mean amplitude from 11.7 ± 1.8 pA to 10.1 ± 1.6 pA, p=0.65, n = 7, student's t-test) (Figure 4A and C). In contrast, the ID-AD1 sample had no effect on the frequency or the amplitude of sEPSCs (mean frequency: from 2.2 ± 0.5 Hz to 2.3 ± 0.7 Hz, mean amplitude: from 9.7 ± 1.7 pA to 10.2 ± 1.4 pA, p=0.45, n = 6, student's t-test) (Figure 4D–F). These results indicate that the AD brain-derived Aβ significantly augments excitatory synaptic input on CA1 pyramidal neurons.

Pyramidal neurons receive both excitatory (sEPSCs) and inhibitory (sIPSCs) inputs, GABAergic axon terminals more easily form synapses with perisomtatic regions of pyramidal cells and strongly influence the output of neurons (DeFelipe, 2002; Garcia-Marin et al., 2009). To record sIPSCs on the same neurons, we adjusted the holding potential to 5 mV, a voltage close to the calculated sEPSCs reverse potential. As shown in Figure 4G–I, the AD1 sample significantly increased inter-event intervals (p=6.19E-6, K-S test) and decreased the frequency of sIPSCs (from 4.7 ± 0.7 Hz to 3.1 ± 0.7 Hz, p=0.008, n = 7, student's t-test), without altering sIPSCs amplitude (from 14.8 ± 1.4 pA to 14.2 ± 0.9 pA, p=0.75, n = 7, student's t-test). In contrast, the ID-AD1 sample had no effect on sIPSCs (frequency: from 5.3 ± 0.4 Hz to 4.8 ± 0.7 Hz, amplitude: from 13.6 ± 1.6 pA to 13.2 ± 2.1 pA, p=0.21, n = 6, student's t-test) (Figure

513 4J-L). These results revealed that brain-derived Aβ significantly reduces GABAergic
514 input on CA1 pyramidal cells.

515 To assess whether the changes of excitatory input (E) and inhibitory input (I) to the
516 same neuron affect the E/I balance of that neuron, we calculated the integrated
517 conductance of sEPSCs and sIPSCs over a 5 minutes period (Figure 4M). Comparison
518 of the integrated conductance before and 30 minutes after AD1 sample application
519 revealed E was increased ~3 fold and I was decreased ~50%, consequently, the E/I
520 balance was increased ~6 fold (n = 7) (Figure 4N). These results show that AD brain-
521 derived Aβ oppositely affects excitatory and inhibitory synaptic transmission, causing an
522 increase in the E/I ratio. These changes, especially the reduction of GABAergic tone on
523 individual neurons, may contribute to neuronal hyperactivity and disturb network
524 homeostasis, thereby perturbing LTP (Wang et al., 2014; Gillespie et al., 2016).

525
526 **Genetic ablation of APP occludes the effects of Aβ on LTP and pre-synaptic**
527 **activity and normalizes the E/I balance**

528 Multiple lines of evidence suggest that the APP may play a role in both GABAergic and
529 glutamatergic neurotransmission (Bai et al., 2008; Kabogo et al., 2010; Pliassova et al.,
530 2016; Schwenk et al., 2016) and separate studies impute a link between Aβ and APP
531 (Lorenzo et al., 2000; Fogel et al., 2014; Kirouac et al., 2017). Thus, having found that
532 brain-derived Aβ acts on pre-synapses and modulates both GABA and glutamate
533 transmission, we investigated if APP was required for these effects. For this, we
534 employed mice null for APP (Figure 5A). In agreement with prior reports, brain slices

from APP KO and WT littermate mice exhibited similar levels of basal activity (p=0.19, One-Way ANOVA) and LTP (Figure 5B and C) (Dawson et al., 1999; Jedlicka et al., 2012). In both WT and APP KO slices treated with the aCSF-B control, TBS induced strong potentiation which lasted the whole recording period (158.1 ± 6.3 % in WT, n = 11, black circles; 151.2 ± 8.5 % in APP KO, n = 9, gray hexagons; F=4.4, p=0.79, comparison of the last 10 minutes of recording using One-Way ANOVA) (Figure 5C and D). In agreement with experiments shown in Figure 2, addition of AD1 extract to WT slices significantly decreased LTP compared to addition of aCSF-B (121.8 ± 5.4 % in WT + AD1, magenta diamonds, n = 7, F=4.5, p=0.0005, WT Ctr vs. WT + AD1, One-Way ANOVA). However, application of the same extract to slices from APP KO mice had no effect on LTP, with the level of LTP in APP KOs indistinguishable from that of WT or APP KO treated with aCSF-B control (145.4 ± 4.2 % in APP KO + AD1, pink upward triangles, F=4.5, p=0.41, APP KO Ctr vs. APP KO + AD1; One-Way ANOVA). Similarly, when applied to APP KO brain slices, AD1 extract had no effect on short-term facilitation (Figure 5E and F).

To assess the generalizability of the rescue of LTP by APP ablation, we tested the effect of an extract from a second AD brain (AD2) on another APP KO mouse line (Zheng et al., 1995). As with the AD1 extract (Figure 2), the AD2 and ID-AD2 extracts were characterized by IP/WB and ELISA. The profiles obtained for AD2 (Figure 6A) were similar to those of AD1 (Figure 2A), except AD2 contained relatively more ~7 kDa species than AD1 (Figure 6 A and B). As seen with the first APP KO line tested (Figure 5), brain slices from the second APP KO line (which we refer to as Zheng APP KOs) (Zheng et al., 1995) exhibited similar levels of basal activity as slices from wild type

mice (F=4.6, *p*=0.91, One-Way ANOVA) (Figure 6E and F). When AD2 extract was applied to slices from WT mice it blocked LTP in an Aβ-dependent fashion (184.1 ± 7.7 % in WT Ctr, black circles, *n* = 12; 137.1 ± 7.2 % in WT + AD2, magenta diamonds, *n* = 12; F=4.96, *p*=0.0001, One-Way ANOVA), but had no effect on LTP elicited from APP KO mice (175.8 ± 9 % in APP KO Ctr, gray hexagons, *n* = 11; 169.9 ± 4 % in APP KO + AD2, pink upward triangles, *n* = 12; F=5.12, *p*=0.56, One-Way ANOVA) (Figure 7A and B).

To further examine whether the APP-dependent block of LTP by AD brain extracts was indeed mediated by Aβ and not some other AW7-reactive material, we tested if the well-established block of LTP mediated by ADDLs (Lambert et al., 1998; Wang et al., 2002; Lauren et al., 2009; Freir et al., 2011) also required expression of APP. ADDLs were prepared as described previously and then assessed using SEC and EM (Figure 6C and D). The ADDL preparation contained a mixture of Aβ aggregates and a small amount of monomer (Figure 6C and D). When applied to brain slices from WT mice, ADDLs (200 nM) blocked LTP (188.9 ± 11.5 % in WT Ctr, black circles, *n* = 8; 123.8 ± 6 % in WT + ADDLs, magenta diamonds, *n* = 6; F=4.75, *p*=0.0007, One-Way ANOVA), but had no effect on LTP elicited from APP KO slices (181.5 ± 15 % in APP KO Ctr, gray hexagons, *n* = 7; 168.1 ± 10 % in APP KO + ADDLs, pink upward triangles, *n* = 7; F=4.85, *p*=0.07, One-Way ANOVA) (Figure 7C and D). Thus, it appears that the well-documented plasticity-disrupting activity of both Aβ extracted from AD brains (Klyubin et al., 2008; Shankar et al., 2008; Barry et al., 2011; Freir et al., 2011; Klyubin et al., 2012)

and synthetic Aβ (Lambert et al., 1998; Wang et al., 2002; Lauren et al., 2009; Freir et al., 2011) require expression of APP.

To investigate whether APP is necessary for the effect of Aβ on the E/I balance (Figure 3), we studied the effects of Aβ on sEPSCs and sIPSCs in brains of Zheng APP KO and WT littermate mice (Figure 8). When applied to WT slices, AD1 extract again increased mean sEPSC frequency (from 2.2 ± 0.1 Hz to 3.4 ± 0.2 Hz, p=0.003, n = 5, student's t-test) and decreased inter-event intervals (p=6.34E-15, K-S test), without altering the amplitude of sEPSCs (mean amplitude: 17.8 ± 0.4 pA vs. 18 ± 1.5 pA, p=0.32, n = 5, student's t-test) (Figure 8A-C); and on the same neuron decreased mean sIPSCs frequency (from 4.2 ± 0.8 Hz to 2.7 ± 0.4 Hz, p=0.006, n = 5, student's t-test) and increased inter-event intervals (p=9.44E-20, K-S test), but not amplitude (mean amplitude from 20 ± 3 pA to 19.3 ± 1.3 pA, p=0.34, n = 5, student's t-test) (Figure 8D-F). These results, which were obtained with WT mice from an entirely different colony as those used in Figure 2, nicely demonstrate the robustness of the Aβ effect (See Figure 4 vs. Figure 8). Most importantly, when AD1 extract was applied to Zheng APP KO slices there was no change in the frequency or amplitude of sEPSCs (mean frequency: from 2.6 ± 0.1 Hz to 2.7 ± 0.4 Hz, mean amplitude: from 15 ± 1.4 pA to 14.6 ± 0.5 pA, p=0.14, K-S test; p=0.26, n = 6, student's t-test) (Figure 8G-I). Similarly, sIPSCs were also unchanged (mean frequency: from 3.5 ± 0.5 Hz to 3.5 ± 0.3 Hz, mean amplitude: from 16.7 ± 1 pA to 16.4 ± 1.6 pA, p=0.58, K-S test; p=0.25, n = 6, student's t-test (Figure 8J-L). Thus, as with our LTP experiments (Figures 5 and 7), ablation of APP completely rescued the effects of Aβ on excitatory and inhibitory input on CA1 pyramidal neurons. Further, since APP KO occluded Aβ alterations on the E and I input at

602 individual neurons, it also prevented Aβ-mediated changes in the integrated
603 conductance of sEPSCs and sIPSCs (Figure 8M). When AD1 extract was applied to
604 WT slices, E increased ~3-fold and I decreased ~44%, resulting in ~5.8-fold increase in
605 the E/I ratio. However, APP KO significantly prevented those E/I ratio changes
606 (p=0.001, E/I in WT vs. E/I in APP KO, One-Way ANOVA) (Figure 8M). These results
607 indicate that APP plays an important role in regulating the acute effects of Aβ on
608 excitatory and inhibitory pre-synaptic release, and consequent maintenance of network
609 homeostasis.

610

611 **Aβ binding to synapses requires APP**

612 To further investigate the targeting of synaptic elements by Aβ and how this might be
613 influenced by APP we used a powerful high-resolution microscopic technique, array
614 tomography (AT), to search for evidence of Aβ binding to synapses in the same brain
615 slices used in our electrophysiology experiments. Upon completion of LTP recording,
616 certain slices from the treatment groups used in Figures 2C and 5C were immediately
617 fixed, processed and used for AT. Sections were stained with 1C22 – the same
618 aggregate-preferring antibody (Mably et al., 2015; Pickett et al., 2016) used in our
619 oAssay, anti-synapsin-1 (for pre-synapses) and anti-PSD95 (for post-synapses).
620 Approximately 7,000 synapses (~3,500 pre-synapses and ~3,500 post-synapses) per
621 slice were analyzed for a total of 100,359 pre-synapses and 99,075 post-synapses. AT
622 revealed, significant anti-Aβ staining at synapse of slices incubated with AD1 extract,
623 with only background staining in samples incubated with aCSF controls and ID-AD1

(Figure 9A-C; Kruskal Wallis test for synapsin-1 ($\chi^2_{(4)}$=10.844, p=0.028), Kruskal Wallis test for PSD95 ($\chi^2_{(4)}$=11.583, p=0.021)). In slices incubated with AD1 extract 1.27 ± 0.47% of pre-synapses and 0.58 ± 0.19% of post-synapses stained with 1C22, whereas in slices that had been incubated with aCSF, only 0.0076 ± 0.013% of pre-synapses and 0.0184 ± 0.087% of post-synapses were 1C22 positive (Dunns *post-hoc* between AD and control for pre-synapses p=0.024 and for post-synapses p=0.010). Slices incubated with extracts immunodepeleted of Aβ exhibited similar background staining with 1C22 as the aCSF control (Figure 9A-C). Thus, the same treatment with AD1 extract that disrupts synaptic plasticity in an Aβ-dependent fashion (Figures 2 and 4) also leads to Aβ binding to synapses (Figure 9A-C). Moreover, the finding that Aβ is present at more pre-synapses than post-synapses (Mann-Whitney U between AD pre-synapses and AD post-synapses U=0, p=0.004) is consistent with our results that suggest a pre-synaptic effect of Aβ (Figures 4 and 8), and with preliminary experiments using an antibody to another pre-synaptic marker, synaptophysin.

The number of Aβ positive synapses detected here is much lower than the amount of Aβ observed at synapses when synthetic oligomers are applied to cultured hippocampal neurons (Lacor et al., 2004; Lacor et al., 2007). However, the current paradigm, of applying soluble AD brain extract to intact mouse brain slices is more relevant to the *in vivo* situation than model systems in which Aβ is applied directly and at high concentrations to dissociated neurons (Lacor et al., 2004; Lacor et al., 2007). Indeed, it is noteworthy that the percentage of synapses positive for Aβ in the current study are consistent with our findings in APP transgenic mouse brain where we observed approximately 1% of postsynaptic densities (PSDs) positive for Aβ distant from plaques

(Koffie et al., 2009). Similarly, in human AD brain at sites distant from plaques, we detected Aβ at 0.6% of PSDs and 0.5% of pre-synaptic terminals (Koffie et al., 2012). Thus, at disease relevant concentrations sufficient to disrupt plasticity, synaptic Aβ binding occurs at levels similar to that observed in human AD brain.

Importantly, when brain slices from APP KO mice were incubated with AD1 extract, little or no synaptic 1C22 staining was detected (Figure 9A-C). These results are notable since expression of APP was found to be required for Aβ-mediated disruption of both long-term plasticity (Figures 5 and 7) and neurotransmitter release (Figure 8). In sum, our AT data are completely congruent with the results of our electrophysiological experiments and indicate that expression of APP is required for the binding and subsequent plasticity-disrupting effects of Aβ, and that these effects are largely mediated on the pre-synapse.

APP mediates binding of synaptotoxic Aβ to brain cells

We reasoned that if synaptotoxic forms of Aβ bound to APP or to an APP containing complex then it should be possible to pre-treat bioactive extracts with a source of APP to deplete the extract of activity. One possible approach would be to add exogenous recombinant APP, but APP is a transmembrane protein and its expression outside of a membrane environment in the absence of proper post-translational modifications precludes its use. Instead, we pre-incubated AD2 extract with either APP-containing (WT) or APP lacking (KO) brain slices (Figure 10A). When AD2 was pre-incubated with

668 WT brain slices and then applied to a fresh WT brain slice it was no longer capable of
669 blocking LTP (216.4 ± 26 % in WT slices + AD2, green upward triangles, *n* = 6; F=4.96,
670 *p*=0.82, One-Way ANOVA) (Figure 10B and C). In contrast, when AD2 extract was pre-
671 incubated with APP KO slices and then applied to a fresh WT brain slice, the AD2
672 extract retained its ability to block LTP (210.3 ± 15 % in WT Ctr, black circles, *n* = 6;
673 146.8 ± 5.4 % in APP KO +AD2, magenta diamonds, *n* = 6; F=4.96, *p*=0.003, One-Way
674 ANOVA, Figure 10B and C). These results are entirely consistent with our array
675 tomography experiments and provide further evidence that APP enables synaptotoxic
676 forms of Aβ to bind to and perturb neurons.

677

678 **Aβ-containing AD brain extract partially blocks LTP in APP hemizygous brain**
679 **slices**

680 To further investigate the requirement of APP for Aβ synaptotoxicity, we tested the
681 effect of AD2 extract on brain slices from APP hemizygous mice. APP expressing wild
682 type C57BL/6 were bred with Zheng APP KO mice and the hemizygous progeny used
683 for LTP experiments. Hemizygous mice express 50% as much APP as WT mice
684 (Figure 11A) and exhibit similar levels of basal activity relative to slices from wild type
685 mice (F=4.6, *p*=0.75, One-Way ANOVA) (Figure 11B). The control level of LTP was
686 also similar in WT and hemizygous brain slices (187.85 ± 5.63 % in WT Ctr, black
687 circles, *n* = 9; 189.69 ± 7.19 % in hemizygous brain slices, gray hexagons, *n* = 9;
688 F=4.45, *p*=0.84, One-Way ANOVA) (Figure 11C and D). When AD2 extract was
689 applied to slices from WT mice it blocked LTP to an extent comparable to that seen in

690 previous experiments (compare Figure 11C and D versus Figure 7A and B) (187.85 ±
691 5.63 % in WT Ctr, black circles, *n* = 9; 136.93 ± 3.14 % in WT + AD2, magenta
692 diamonds, *n* = 10; F=4.5, *p*=2.67E-007, One-Way ANOVA). Similarly, AD2 extract
693 impaired LTP in APP hemizygous mice (189.69 ± 7.19 % in APP +/- Ctr, gray hexagons,
694 *n* = 9; 154.83 ± 6 % in APP +/- AD2, pink upward triangles, *n* = 10; F=4.49, *p*=0.003,
695 One-Way ANOVA) (Figure 11C and D). Although the extent of the block in hemizygous
696 slices was somewhat reduced compared WT slices (F=4.45, *p*=0.84, Control in WT
697 mice vs. Control in APP +/- mice; F=4.5, *p*=2.67E-007, Control vs. AD2 in WT mice;
698 F=4.49, *p*=0.003, Control vs. AD2 in WT mice; One-Way ANOVA), the effect of AD2
699 extract on hemizygous brain slices stands in contrast to its lack of effect on APP KO
700 slices (Figure 7A and B). The partial attenuation of Aβ synaptotoxicity in APP
701 hemizygous brain indicates a gene-dose effect, such that 50% of the normal level of
702 APP is sufficient to mediate some block of LTP, but not the full block of LTP seen in
703 APP WT mice. Further studies will be required to determine the minimal reduction in
704 APP levels that allows full protection against the plasticity disrupting effects of Aβ.

705

Discussion

To better understand how Aβ disrupts synaptic plasticity we combined the use of the most disease relevant form of Aβ, material extracted from human AD brain, with electrophysiological approaches and high-resolution microscopy. Consistent with prior studies, we show that extracts from the brains of individuals who died with AD block LTP (Shankar et al., 2008; Barry et al., 2011; Freir et al., 2011; Yang et al., 2017). We further show that, concomitant with the block of LTP, there is an increase in pre-synaptic release and disruption of E/I balance. In accord with these synaptic effects of Aβ, we demonstrate that exogenously applied AD brain-derived Aβ binds to synapses, with more Aβ oligomers detected on pre-synapses than on the post-synapses. Our finding that treatment with brain-derived Aβ enhances excitatory drive agrees well with studies showing that aggregated forms of synthetic Aβ increase EPSPs, action potentials, and membrane depolarizations (Hartley et al., 1999; Minkeviciene et al., 2009; Kurudenkandy et al., 2014). Our study is unique in that we employed brain-derived Aβ, and that the concentration of this material was much lower than the synthetic Aβ used in prior studies. In support of the strength of this experimental paradigm, the levels of synaptic Aβ we observe in this study are very similar to those observed with array tomography in our studies of human AD brain (Koffie et al., 2012).

The apparent paradox that ectopic application of Aβ causes a net increase in excitation, yet impairs LTP may result because of glutamate spillover and activation of extra- or perisynaptic NR2B-enriched NMDARs, which play a major role in LTD induction (Li et al., 2011; Zhang et al., 2016). In such a scenario, synaptic depression may result from an initial increase in synaptic activation of NMDARs by glutamate, followed by synaptic

NMDAR desensitization, NMDAR/AMPAR internalization, and activation of extrasynaptic NMDARs and mGluRs (Born et al., 2014). However, it is unclear why ablation of APP could recover such effects.

An alternative explanation that accounts for a role for APP in the impairment of post-synaptic efficacy is that exogenous AD brain-derived soluble aggregates and endogenously produced monomer have differential effects. Aβ is known to be released in an activity-dependent manner (Kamenetz et al., 2003; Cirrito et al., 2005), whereas elevated Aβ levels result in depressed glutamatergic synaptic transmission and glutamate receptor endocytosis (Kamenetz et al., 2003; Hsieh et al., 2006). Thus, it is plausible that the increase in glutamate release induced by soluble Aβ aggregates may also lead to an increase in *de novo* Aβ monomer production and this in turn may depress post-synaptic activity. Such a scenario would necessarily require expression of endogenous APP and explain why ablation of APP can obviate the block of LTP caused by brain-derived soluble Aβ aggregates. The fact that Aβ treated APP hemizygous slices exhibited an attenuated block is consistent with a partial reduction in the amount of endogenous Aβ. With regard to the protection of LTP upon ablation of APP, it is important to emphasize the robust nature and generalizability of this phenomenon. We observed the same protection using two different APP KO mouse lines (Zheng et al., 1995; Callahan et al., 2017), extracts from 2 different AD brains, and synthetic Aβ oligomers. Both AD extracts blocked LTP in an Aβ-dependent manner when applied to wild type mouse brain slices, but the same AD extracts had no effect on LTP elicited from APP KO slices. Moreover, the extent of Aβ binding to synapses was similar in two

751 different sources of wild type mice (Figure 7B and C), and the pattern observed was
752 reminiscent of that seen in AD brain (Pickett et al., 2016).
753 There is evidence that APP can act as a receptor for Aβ (Melchor and Van Nostrand,
754 2000; Van Nostrand et al., 2002; Yankner and Lu, 2009; Fogel et al., 2014; Kirouac et
755 al., 2017) and that APP may mediate increased excitatory drive (Fogel et al., 2014).
756 Specifically, Aβ was unable to promote aberrant neurotransmitter release in the
757 absence of APP (Fogel et al., 2014). Our findings that binding of soluble Aβ aggregates
758 to synapses requires expression of APP and that synaptotoxic Aβ can be bound by APP
759 expressing, but not APP lacking brain tissue, are consistent, but not proof, that APP
760 may act as a receptor for Aβ. In this regard, it is worth noting that APP is known to both
761 regulate L-type calcium channels in GABAergic neurons, interact with the pore-forming
762 subunit Cav1.2 (Yang et al., 2009), and is a member of the $GABA_B$-R receptor complex
763 (Schwenk et al., 2016). In addition, there is evidence from proteomic studies indicating
764 that APP interacts with more than 30 different proteins including proteins key to synaptic
765 vesicle turnover (Kohli et al., 2012; Del Prete et al., 2014; Lassek et al., 2014; Wilhelm
766 et al., 2014), and proteins (such as the prion protein) implicated in binding Aβ (Bai et al.,
767 2008; Lauren et al., 2009). Thus, Aβ could exert an APP-dependent effect either by
768 directly binding to APP or binding to protein complexes of which APP is a component
769 and stabilizing member. The APP gene-dose dependent response to Aβ that we
770 observed is equally compatible with direct or indirect binding to APP.
771 So far we have considered the effects of Aβ on synapses and a single hippocampal
772 pathway (the *Schaffer Collateral*), but Aβ is also thought to have network-wide effects
773 (Palop and Mucke, 2010). For instance, Aβ-induced increases in excitatory network

activity could lead to synaptic depression through homeostatic mechanisms. It is well established that acute treatment of primary neurons with bicuculline (a $GABA_A$ antagonist) increases overall neuronal activity and firing rates (Vertkin et al., 2015). However, after a few days, neuronal activity returns to control levels. By analogy, it is reasonable that the disruption of E/I balance seen with our acute Aβ treatment may also cause both short-term local and long-lasting network effects. Given the fact that Aβ treatment increases excitatory drive and decreases inhibitory drive, and that GABA-ergic interneurons express high levels of APP in DG (Wang et al., 2014; Del Turco et al., 2016) it is tempting to speculate that Aβ-mediated disruption of GABA-ergic interneurons may play a critical role in the cognitive impairment that occurs early in AD (Gillespie et al., 2016). Clearly, further studies will be required to delineate the influence of APP on both network regulation and other forms of synaptic plasticity, such as LTD.

Considerable data from the study of APP transgenics implicate impairment of GABAergic interneurons as central to the network disturbances evident in these models (Busche and Konnerth, 2015; Palop and Mucke, 2016). However, the unphysiological expression of high levels of APP and the concomitant release of Aβ from the expressed transgene make it difficult to differentiate between effects mediated by Aβ versus APP, or non-Aβ APP metabolites (Melnikova et al., 2013; Born et al., 2014; Fowler et al., 2014). Nonetheless, growing evidence suggests that GABAergic interneurons play a prominent role in homeostatic regulation of hippocampal networks, and there is compelling proteomic and physiological data that link APP and $GABA_{B1a}$-R (Wang et al., 2014; Gillespie et al., 2016; Schwenk et al., 2016). Consequently, further investigations on how Aβ effects $GABA_B$-R expression, $GABA_B$-R-APP interactions and whether

797 $GABA_B$-R KOs are resistant to Aβ are merited and may lead to a pharmacological
798 means to attenuate Aβ synaptotoxicity. Similarly, modulation of APP expression may
799 also offer therapeutic potential. However, while our results demonstrate that ablation of
800 APP in brain slices from young (2-3 months) mice protects against the acute
801 synaptotoxicity of Aβ, widespread knock-out of APP is not recommended. APP appears
802 to be involved in many physiological processes (Yang et al., 2009; Muller and Zheng,
803 2012; Del Prete et al., 2014; Lassek et al., 2014; Wang et al., 2014) and aged APP null
804 mice exhibit hypersensitivity to kainate-induced seizures (Steinbach et al., 1998),
805 altered exploratory behavior, deficits in spatial memory, and impairment of LTP
806 (Dawson et al., 1999; Seabrook et al., 1999; Ring et al., 2007). No such deficits have
807 been reported in APP hemizygous mice. Thus, it may be possible to down regulate APP
808 expression so as to maintain normal function, yet attenuate Aβ synaptotoxicity.
809 However, hemizygous reduction of APP allows only partial protection against the
810 plasticity disrupting effects of Aβ, and further studies will be required to determine the
811 minimal reduction in APP levels that allows a more fulsome protection.

812

Figure Legends

Figure 1. Processing of array tomography images.

Fields of 10 μm by 10 μm are cropped from an image stack, these are then made into binary stacks in image J and processed in MATLAB to remove objects not found in serial slices. Scale bar is 2 μm.

Figure 2. The water-soluble extract of AD brain, but not normal control, contains both Aβ monomers and oligomers and perturbs long-term synaptic plasticity.

(A) Aqueous extract of AD1 was treated with either pre-immune rabbit serum or with AW7 antiserum. Portions of the mock immunodepleted sample (AD1, magenta) and the AW7 immunodepleted sample (ID-AD1, green) were then analyzed by IP/WB, using AW7 for IP and a combination of 2G3 and 21F12 (left panel), or 6E10 (right panel) for WB. **M** denotes Aβ monomer and ⁎ indicates a broad smear ~7–8 kDa. Synthetic Aβ1-42, -31Aβ40 and Aη–α each at 2 ng/lane were used as controls. As expected 6E10 detected all 3 synthetic peptides, whereas 2G3/21F12 detected Aβ1-42, -31Aβ40 but not Aη–α. Only non-specific (NS) bands were detected above 16kDa marker. **(B)** AD1 (magenta) and ID-AD1 (green) samples were incubated +/- 5 M GuHCl and analyzed using immunoassays that preferentially recognize Aβ oligomers (1C22-3D6b, left panel) or Aβ42 monomer (266-21F12b, right panel). Values shown are the mean ± SEM of duplicate measurements and are representative of 2 separate experiments. **(C)** Time course plots show that the AD sample but not the ID-AD sample blocked hippocampal LTP. The gray horizontal bar indicates the time period when sample was present in the bath. 1, 2, indicate example traces from time points just prior to the theta burst stimulation (↑↑↑ TBS) (1) and 60 minutes after TBS (2), respectively. The aCSF control is shown in black circles; AD treatment is shown in magenta diamonds and ID-AD with green downward triangles. Each slice used for each treatment was from a different animal. Scale bar 0.2 mV, 10 milliseconds. **(D)** Histogram plots of the average

potentiation for the last 10 minutes of traces shown in **C**. Treatment of slices with AD1 sample significantly inhibited LTP compared to the aCSF vehicle control (F=4.26，*p*=6.98E-9) and ID-AD1 treatment (F=4.14, *p*=3.56E-12); in contrast ID-AD1 had no effect on LTP relative to the vehicle control (F=4.23, *p*=0.12, One-Way ANOVA). Symbols are the same as in panel **C**. (**E**) Time course plots show that the brain extract from a cognitively intact non-AD control (NC) did not blocked hippocampal LTP. The gray horizontal bar indicates the time period when sample was present in the bath. 1, 2, indicate example traces from time points just prior to the theta burst stimulation (↑↑↑ TBS) (1) and 60 minutes after TBS (2), respectively. The aCSF control is shown in black circles; NC treatment is shown in gray hexagons. Each slice used for each treatment was from a different animal. Scale bar 0.5 mV, 10 milliseconds. **(F)** Histogram plots of the average potentiation for the last 10 minutes of traces shown in **E** and average of last 10 minutes from individual experiment in every group. Treatment of slices with NC sample did not inhibited LTP compared to the aCSF vehicle control (F=4.6, *p*=0.95, One-Way ANOVA). Symbols are the same as in panel **E**. Values shown are the mean ± SEM. ### *p*<0.001

Figure 3. The Aβ-containing water-soluble extract of AD1 perturbs short-term facilitation.

(**A**) Representative traces of averaged field recordings were collected after 5 stimulation bursts (inter-stimulation interval 20 milliseconds, inter-burst interval 30 seconds) before (black, aCSF) and 30 minutes after perfusion with the AD1 sample (magenta). The trace shown for the AD1 samples are scaled so that the first response matches that of the aCSF control. Scale bars: 0.5 mV, 10 milliseconds. (**B**) fEPSPs amplitude after 2 to 5 stimulations were normalized to the value obtained after the first stimulation. Compared to vehicle control, AD1 treatment induced a small but significant decrease in short-term synaptic facilitation, (p=0.02) after the 3rd, (p=0.004) the 4th stimulation and 5th stimulation (p=0.004); n = 6, student's t-test. Values shown are the mean ± SEM. # p< 0.05; ## p<0.01. (**C**) Representative traces of averaged field recordings were collected after 5 stimulation bursts (inter-stimulation interval 20 milliseconds, inter-burst interval 30 seconds) before (black, aCSF) and 30 minutes after perfusion with the ID-AD1 sample (green). Scale bars: 0.4 mV, 10 milliseconds. ID-AD1 treatment did not affect short-term synaptic facilitation (n = 5, F=5.32, p=0.91, One-Way ANOVA).

Figure 4. AD brain-derived Aβ affects both excitatory and inhibitory synaptic inputs, causing disruption of the excitatory/inhibitory ratio at individual CA1 neurons.

(**A, D**) Example traces of spontaneous excitatory post-synaptic currents (sEPSCs) before (aCSF, black) and 30 minutes after addition of sample (AD1, magenta; ID-AD1, green) recorded from individual pyramidal neurons in the hippocampal CA1 area of brain slices with the holding potential fixed at -70 mV. Scale bars: 20 pA, 700 millisecond. (**B**) 30 minutes of AD1 treatment decreased cumulative distributions of inter-event intervals and increased mean frequency (insert) (p=1.65E-6, K-S test; p< 0.02, student's t-test; n = 7), but (**C**) did not change the cumulative distributions or the mean value (insert) of the amplitude of sEPSCs (n = 7). (**E, F**) The ID-AD1 sample had no effect on either frequency or amplitude of sEPSCs (n = 6). (**G, J**) Example traces of spontaneous inhibitory post-synaptic currents (sIPSCs) before (aCSF, black) and 30 minutes after treatment (AD1, magenta; ID-AD1, green) were recorded on the same individual pyramidal neurons upon increasing the holding potential to 5 mV. Scale bars: 20 pA, 700 milliseconds. (**H**) 30 minutes of treatment with the AD1 sample increased inter-event intervals and decreased mean frequency (insert) of sIPSCs (magenta) versus aCSF (black) (p=6.19E-6, K-S test; p=0.008, student's t-test; n = 7). (**I**) Treatment with the AD1 sample did not affect the amplitude of sIPSCs (n = 7) and the ID-AD1 sample had no effect on frequency (**K**) or the amplitude (**L**) of sIPSCs versus aCSF control (n = 7). **(M)** Representative traces of sIPSCs and sEPSCs from the same pyramidal neuron show charge transfer measured as the area of events above threshold in the aCSF control. Scale bars: 10 pA, 200 milliseconds. **(N)** Integrated

conductances measured between 30 - 35 minutes after addition of AD1 application were normalized to the value of 5 minutes before addition of AD1. Mean excitatory integrated conductance increased and mean inhibitory integrated conductance decreased upon treatment of AD1 (E: excitatory input/sEPSCs; I: inhibitory input/sIPSCs). Each slice used for each treatment was from a different animal. # $p < 0.05$, ## $p < 0.01$.

Figure 5. Expression of APP is required for the plasticity-disrupting activity of Aβ-containing AD brain extract.

(A) Detergent extracts of mouse brain slices used for electrophysiology were analyzed for APP by Western blotting with 22C11. Full-length APP was readily detected in extracts from wild type littermate mice (WT) but not APP knockout mice (APP KO). Slices from 2 APP KO mice (KO1 and KO2) and 2 WT mice (WT1 and WT2) are shown. **(B)** Input/output curves recorded in the hippocampal CA1 area are highly similar for both WT and APP KO mouse brain slices (p=0.19, One-Way ANOVA). Values are mean ± SEM. **(C)** LTP recorded in hippocampal CA1 was similar in brain slices from WT and APP KO mice (WT Ctr, black circles vs. APP KO Ctr, gray hexagons, p=0.79, comparison of the last 10 minutes recording using One-Way ANOVA). However, the extract from AD1 brain blocked LTP in WT but not in APP KO mice brain slices. Horizontal gray bar indicates the duration in which sample was present. 1 and 2 indicate example traces from time points just prior to the theta burst stimulation (↑↑↑ TBS) (1) and 60 minutes after TBS (2), respectively. The aCSF control in WT mice is shown with black circles; AD1 treatment in WT mice is shown in magenta diamonds; the aCSF control in APP KO mice is shown in gray hexagons and AD1 treatment in APP KO mice is shown using pink upward triangles. WT slices for each treatment came from different animals; the APP KO slices came from a total of 4 APP KO mice. Scale bars: 0.5 mV, 15 milliseconds. **(D)** Comparison of average potentiation from last 10 minutes of LTP recording (F=4.5, p=0.0005, Control vs. AD1 in WT mice; F=4.5, p=0.41, Control vs. AD1 in APP KO mice; One-Way ANOVA). Symbols correspond to those in panel **C**. (**E**) Representative traces of averaged field recordings were collected after 5 stimulation

bursts (inter-stimulation interval 20 millisecond, inter-burst interval 30 seconds) before (gray, aCSF) and 30 minutes after perfusion with the AD1 sample (pink) on brain slices from APP KO mouse. Scale bars: 0.5 mV, 10 millisecond. (**F**) fEPSPs amplitude after 2 to 5 stimulations were normalized to the value obtained after the first stimulation. There is no significant difference between aCSF control and the presence of AD1 brain extract application (n = 5, F=5.32, p=0.7, One-Way ANOVA). Values are mean ± SEM. Each slice used for each treatment was from a different animal. ### p<0.001.

Figure 6. Characterization of the aqueous extract from AD2 brain, synthetic Aβ oligomers, and second APP KO mouse line. **(A)** Aqueous extract of AD2 was treated with either pre-immune serum or with AW7 antiserum. Portions of the mock immunodepleted sample (AD2, magenta) and the AW7 immunodepleted sample (ID-AD2, green) were then analyzed by IP/WB, using AW7 for IP and a combination of 2G3 and 21F12 (left panel), or 6E10 (right panel) for WB. As expected, recombinant Aη–α was detected by 6E10, but not 2G3/21F12. **M** denotes Aβ monomer and ⁎ indicates a broad smear ~7–8 kDa. Only non-specific (NS) bands were detected above 16 kDa marker. (**B)** AD2 (magenta) and ID-AD2 (green) samples were incubated +/- 5 M GuHCl and analyzed using an immunoassay that preferentially recognizes Aβ42 monomer (266-21F12b). AW7 ID reduced monomer from 6.65 ± 0.01 ng/ml to undetectable level without GuHCl treatment. Upon treatment with GuHCl, the amount of Aβ42 increased to 46.94 ± 0.2 ng/ml in AD2 and this was reduced to 8.62 ± 0.1 ng/ml by immunodepletion. (**C**) Size-exclusion chromatography of ADDLs revealed a prominent high molecular weight peak, a trail of intermediate molecular weight species and a small Aβ monomer peak. (**D**) Negative contrast electron micrograph shows mostly protofibril-like structures. Scale bar is 50 nm. **(E)** Brain slices from wild type (WT) and a second line of APP knock-outs (KO) were analyzed for APP by Western blotting with 22C11. Full-length APP was readily detected in extracts from WT but not APP KO. Slices from 2 KO (KO1 and KO2) and 2 WT (WT1 and WT2) mice are shown. **(F)** Input/output curves recorded in the hippocampal CA1 area are highly similar for WT and APP KO mouse brain slices ($F=4.6$, $p=0.91$, One-Way ANOVA). Values are mean ± SEM. Each slice used for each treatment was from a different animal.

Figure 7. A second APP KO mouse line confirms that APP is required for the synaptic-disrupting activity of both AD brain and synthetic Aβ oligomers.

(A) LTP recorded in hippocampal CA1 was similar in brain slices from WT and Zheng APP KO mice. Notably, the extract from AD2 blocked LTP in brain slices from WT but not APP KO mice. Horizontal gray bar indicates the duration during when sample was present. 1 and 2 indicate example traces from time points just prior to the theta burst stimulation (↑↑↑ TBS) (1) and 60 minutes after TBS (2), respectively. The aCSF control in WT mice is shown with black circles; AD2 treatment in WT mice is shown in magenta diamonds; ID-AD2 treatment in WT slices in green downward triangles. The aCSF control in APP KO mice is shown in gray hexagons and AD2 treatment in APP KO mice is shown using pink upward triangles. WT slices for each treatment came from different animals; the APP KO slices came from a total of 6 APP KO mice. Scale bars: 0.5 mV, 15 millisecond. **(B)** Comparison of average potentiation from last 10 minutes of LTP recording (F=4.96, *p*=0.0001, Control vs. AD2 in WT mice; F=5.12, *p*=0.56, Control vs. AD2 in APP KO mice; One-Way ANOVA). Symbols correspond to those in panel **A**. **(C)** ADDLs blocked LTP in WT, but not in APP KO, brain slices. Horizontal gray bar indicates the duration during when sample was present. 1 and 2 indicate example traces from time points just prior to the theta burst stimulation (↑↑↑ TBS) (1) and 60 minutes after TBS (2), respectively. The aCSF WT slices control is shown with black circles; WT slices treated with ADDLs is in magenta diamonds; and vehicle in green downward triangles. The aCSF control in APP KO mice is shown in gray hexagons and ADDLs treatment in APP KO mice is shown using pink upward triangles. WT slices for

each treatment came from different animals; the APP KO slices came from a total of 6 APP KO mice. Scale bars: 0.7 mV, 15 millisecond. **(D)** Comparison of average potentiation from last 10 minutes of LTP recording (F=4.75, *p*=0.0006, Control vs. ADDLs in WT mice; F=4.75, *p*=0.93, Control vs. vehicle in WT mice; F=4.84, *p*=0.07, Control vs. ADDLs in APP KO mice; One-Way ANOVA). Symbols correspond to those in panel **C**. Each slice used for each treatment was from a different animal. ### *p*< 0.001.

Figure 8. APP knock out occludes the effects of Aβ-containing AD brain extract on both excitatory and inhibitory post-synaptic currents and rescues the disruption of E/I balance.

(A, D) Example traces of sEPSCs **(A)** and sIPSCs **(D)** before (aCSF, black) and 30 minutes after addition of AD1 extract (magenta) on WT hippocampal brain slices. Scale bars: 20 pA, 700 millisecond. **(B)** Treatment with AD1 extract decreased inter-event intervals and increased mean frequency (insert) of sEPSCs (p=6.34E-15, K-S test; p=0.003, student's t-test; n = 5), but **(C)** did not significantly change the cumulative distributions or the mean value (insert) of the amplitude of sEPSCs (n = 5) on WT slices. **(E)** 30 minutes of AD1 treatment increased inter-event intervals and decreased mean frequency (insert) of sIPSCs (p=9.44E-20, K-S test; p=0.006, student's t-test; n = 5), but **(F)** did not affect the cumulative distributions or the mean value (insert) of the amplitude of sIPSCs (n = 5) on WT slices. (**G, J)** Example traces of spontaneous post-synaptic currents (sEPSCs, **G**; sIPSCs, **J**) before (aCSF, gray) and 30-40 minutes following addition of AD1 extract (pink) on APP KO mice hippocampal brain slices. Scale bars: 20 pA, 700 millisecond. (**H**) Treatment with AD1 sample affected neither frequency nor amplitude (I) of sEPSCs (p=0.14, K-S test; p=0.26, student's t-test; n = 6) on APP KO mice. Similarly, treatment of APP KO neurons with AD1 did not change frequency (**K**) or the amplitude (**L,** p=0.58, K-S test; p=0.25 student's t-test; n = 6) of sIPSCs. **(M)** Application of Aβ-containing AD brain extract significantly changed the integrated conductance of both excitatory (E) and inhibitory (I) input to neurons and disrupted the E/I balance in WT animals, but not in APP KO mice (p=0.001, E/I in WT vs. E/I in APP KO, One-Way ANOVA).

Figure 9: Aβ binding to synaptic terminals requires expression of APP.

(**A**) Array tomography of hippocampi stained for synapsin-1 (pre-synapses), Aβ (1C22), and PSD95 (post-synapses) reveal co-localization of Aβ at synapses in slices incubated with AD1 brain extract. Images have been processed for analysis as described in the methods and Figure 1. (**B** and **C**) The amount of synaptic 1C22 staining was significantly greater in slices incubated with AD1 extract than in slices incubated with aCSF or ID-AD1 extract based on (**B**) co-localization of 1C22 and synapsin 1 staining (Kruskal Wallis test ($\chi^2_{(4)}$=10.844, p=0.028) Dunns *post-hoc* vs. control p=0.021), and (**C**) 1C22 and PSD95 co-localization (Kruskal Wallis test for PSD95 ($\chi^2_{(4)}$=11.583, p=0.021; Dunns *post-hoc* vs. control, p=0.01). Importantly, when slices from APP KO mice were incubated with AD1 extract there was no significant co-localization of 1C22 staining with either synapsin 1 (**B**) (Dunns *post-hoc* vs. control, p=1.000) or PSD-95 (**C**) (Dunns *post-hoc* vs. control, p=1.000). Graphs represent the medians ± the interquartile range per treatment. Each data point is derived from the analysis of ~3,500 synapses imaged per brain slice. Within each treatment group the 3 slices used were from 3 different mice (**B** and **C**). Arrows indicate specific examples of 1C22 staining co-localizing with pre- or post-synapses. Scale bar is 2 μm in (**A**). # p< 0.05.

Figure 10. APP expressing, but not APP lacking, brain slices bind synaptotoxic Aβ.

(A) AD2 brain extract was pre-incubated with either 4 WT or 4 APP KO brain slices for 2 hours and the resultant solutions were used to perfuse WT brain slices. **(B)** Time course plots of LTP recorded in WT brain hippocampal CA1 show that AD2 brain extract pre-incubated with APP KO brains slices blocked LTP, whereas AD2 pre-incubated with WT brain slices allow normal LTP. Horizontal gray bar indicates the duration during when sample was present. 1and 2 indicate example traces from time points just prior to the theta burst stimulation (↑↑↑ TBS) (1) and 60 minutes after TBS (2), respectively. The aCSF control in WT mice is shown with black circles; AD2 incubated with APP KO brain slices in WT mice is shown in magenta diamonds; AD2 pre-incubated with WT brain slices is in green downward triangles. Scale bars: 0.5 mV, 15 millisecond. **(C)** Comparison of average potentiation from last 10 minutes of LTP recording ($F=4.96$, $p=0.003$, Control vs. APP KO slices with AD2; $F=4.96$, $p=0.82$, Control vs. WT slices with AD2; One-Way ANOVA). Symbols correspond to those in panel **B**. Each slice used for recording for each treatment was from a different animal. ## $p<0.005$.

Figure 11. The level of APP expression influences the plasticity-disrupting activity of Aβ-containing AD brain extract.

(A) Detergent extracts of from WT, APP +/- and APP -/- mouse brain slices used for electrophysiology were analyzed for APP by Western blotting with 22C11. Full-length APP was readily detected in extracts from wild type mice (WT) and APP +/- mice, but not APP -/- mice. Ten μg total protein from APP +/- slices contained a similar amount of APP as 5 μg total protein from WT slices. **(B)** Input/output curves recorded in the hippocampal CA1 area are highly similar for both WT and APP +/- mouse brain slices (F=4.6, *p*=0.75, One-Way ANOVA). **(C)** LTP recorded in hippocampal CA1 was similar in brain slices from WT and APP +/- mice. However, AD2 caused a stronger block of LTP in WT slices compared with APP +/- slices. Horizontal gray bar indicates the duration during when sample was present. 1 and 2 indicate example traces from time points just prior to the theta burst stimulation (↑↑↑ TBS) (1) and 60 minutes after TBS (2), respectively. The aCSF control in WT mice is shown with black circles; AD2 treatment in WT mice is shown in magenta diamonds; the aCSF control in APP +/- mice is shown in gray hexagons and AD2 treatment in APP +/- mice is shown using pink upward triangles. Scale bars: 0.5 mV, 15 milliseconds. Each slice used for each treatment was from a different animal. **(D)** Comparison of average potentiation from the last 10 minutes of LTP recording (F=4.45, *p*=0.84, Control in WT mice vs. Control in APP +/- mice; F=4.5, *p*=2.67E-007, Control vs. AD2 in WT mice; F=4.49, *p*=0.003, Control vs. AD2 in WT mice; One-Way ANOVA). Symbols correspond to those in panel

C. Values are mean ± SEM. Each slice used for each treatment was from a different animal. ## $p<0.005$, ### $p<0.0001$.

References

Abramov E, Dolev I, Fogel H, Ciccotosto GD, Ruff E, Slutsky I (2009) Amyloid-beta as a positive endogenous regulator of release probability at hippocampal synapses. Nat Neurosci 12:1567-1576.

Bai Y, Markham K, Chen F, Weerasekera R, Watts J, Horne P, Wakutani Y, Bagshaw R, Mathews PM, Fraser PE, Westaway D, St George-Hyslop P, Schmitt-Ulms G (2008) The in vivo brain interactome of the amyloid precursor protein. Mol Cell Proteomics 7:15-34.

Barry AE, Klyubin I, Mc Donald JM, Mably AJ, Farrell MA, Scott M, Walsh DM, Rowan MJ (2011) Alzheimer's disease brain-derived amyloid-beta-mediated inhibition of LTP in vivo is prevented by immunotargeting cellular prion protein. J Neurosci 31:7259-7263.

Betts V, Leissring MA, Dolios G, Wang R, Selkoe DJ, Walsh DM (2008) Aggregation and catabolism of disease-associated intra-Abeta mutations: reduced proteolysis of AbetaA21G by neprilysin. Neurobiol Dis 31:442-450.

Borlikova GG, Trejo M, Mably AJ, Mc Donald JM, Sala Frigerio C, Regan CM, Murphy KJ, Masliah E, Walsh DM (2013) Alzheimer brain-derived amyloid beta-protein impairs synaptic remodeling and memory consolidation. Neurobiol Aging 34:1315-1327.

Born HA, Kim JY, Savjani RR, Das P, Dabaghian YA, Guo Q, Yoo JW, Schuler DR, Cirrito JR, Zheng H, Golde TE, Noebels JL, Jankowsky JL (2014) Genetic suppression of transgenic APP rescues Hypersynchronous network activity in a mouse model of Alzeimer's disease. J Neurosci 34:3826-3840.

Busche MA, Konnerth A (2015) Neuronal hyperactivity--A key defect in Alzheimer's disease? Bioessays 37:624-632.

Callahan DG, Taylor WM, Tilearcio M, Cavanaugh T, Selkoe DJ, Young-Pearse TL (2017) Embryonic mosaic deletion of APP results in displaced Reelin-expressing cells in the cerebral cortex. Dev Biol 424:138-146.

Cirrito JR, Yamada KA, Finn MB, Sloviter RS, Bales KR, May PC, Schoepp DD, Paul SM, Mennerick S, Holtzman DM (2005) Synaptic activity regulates interstitial fluid amyloid-beta levels in vivo. Neuron 48:913-922.

Cleary JP, Walsh DM, Hofmeister JJ, Shankar GM, Kuskowski MA, Selkoe DJ, Ashe KH (2005) Natural oligomers of the amyloid-beta protein specifically disrupt cognitive function. Nat Neurosci 8:79-84.

Conboy L, Murphy KJ, Regan CM (2005) Amyloid precursor protein expression in the rat hippocampal dentate gyrus modulates during memory consolidation. J Neurochem 95:1677-1688.

Dawson GR, Seabrook GR, Zheng H, Smith DW, Graham S, O'Dowd G, Bowery BJ, Boyce S, Trumbauer ME, Chen HY, Van der Ploeg LH, Sirinathsinghji DJ (1999) Age-related cognitive deficits, impaired long-term potentiation and reduction in synaptic marker density in mice lacking the beta-amyloid precursor protein. Neuroscience 90:1-13.

De Strooper B (2010) Proteases and proteolysis in Alzheimer disease: a multifactorial view on the disease process. Physiol Rev 90:465-494.

DeFelipe J (2002) Cortical interneurons: from Cajal to 2001. Prog Brain Res 136:215-238.

Del Prete D, Lombino F, Liu X, D'Adamio L (2014) APP is cleaved by Bace1 in pre-synaptic vesicles and establishes a pre-synaptic interactome, via its intracellular domain, with molecular complexes that regulate pre-synaptic vesicles functions. PLoS One 9:e108576.

Del Turco D, Paul MH, Schlaudraff J, Hick M, Endres K, Muller UC, Deller T (2016) Region-Specific Differences in Amyloid Precursor Protein Expression in the Mouse Hippocampus. Front Mol Neurosci 9:134.

Doyle E, Bruce MT, Breen KC, Smith DC, Anderton B, Regan CM (1990) Intraventricular infusions of antibodies to amyloid-beta-protein precursor impair the acquisition of a passive avoidance response in the rat. Neurosci Lett 115:97-102.

Fanutza T, Del Prete D, Ford MJ, Castillo PE, D'Adamio L (2015) APP and APLP2 interact with the synaptic release machinery and facilitate transmitter release at hippocampal synapses. Elife 4:e09743.

Fogel H, Frere S, Segev O, Bharill S, Shapira I, Gazit N, O'Malley T, Slomowitz E, Berdichevsky Y, Walsh DM, Isacoff EY, Hirsch JA, Slutsky I (2014) APP homodimers transduce an amyloid-beta-mediated increase in release probability at excitatory synapses. Cell Rep 7:1560-1576.

Fowler SW, Chiang AC, Savjani RR, Larson ME, Sherman MA, Schuler DR, Cirrito JR, Lesne SE, Jankowsky JL (2014) Genetic modulation of soluble Abeta rescues cognitive and synaptic impairment in a mouse model of Alzheimer's disease. J Neurosci 34:7871-7885.

Freir DB, Nicoll AJ, Klyubin I, Panico S, Mc Donald JM, Risse E, Asante EA, Farrow MA, Sessions RB, Saibil HR, Clarke AR, Rowan MJ, Walsh DM, Collinge J (2011) Interaction between prion protein and toxic amyloid beta assemblies can be therapeutically targeted at multiple sites. Nat Commun 2:336.

Garcia-Marin V, Blazquez-Llorca L, Rodriguez JR, Boluda S, Muntane G, Ferrer I, Defelipe J (2009) Diminished perisomatic GABAergic terminals on cortical neurons adjacent to amyloid plaques. Front Neuroanat 3:28.

Gillespie AK, Jones EA, Lin YH, Karlsson MP, Kay K, Yoon SY, Tong LM, Nova P, Carr JS, Frank LM, Huang Y (2016) Apolipoprotein E4 Causes Age-Dependent Disruption of Slow Gamma Oscillations during Hippocampal Sharp-Wave Ripples. Neuron 90:740-751.

Guerreiro R, Hardy J (2014) Genetics of Alzheimer's disease. Neurotherapeutics 11:732-737.

Hartley DM, Walsh DM, Ye CP, Diehl T, Vasquez S, Vassilev PM, Teplow DB, Selkoe DJ (1999) Protofibrillar intermediates of amyloid beta-protein induce acute electrophysiological changes and progressive neurotoxicity in cortical neurons. J Neurosci 19:8876-8884.

Hsieh H, Boehm J, Sato C, Iwatsubo T, Tomita T, Sisodia S, Malinow R (2006) AMPAR removal underlies Abeta-induced synaptic depression and dendritic spine loss. Neuron 52:831-843.

Huang JK, Ma PL, Ji SY, Zhao XL, Tan JX, Sun XJ, Huang FD (2013) Age-dependent alterations in the presynaptic active zone in a Drosophila model of Alzheimer's disease. Neurobiol Dis 51:161-167.

Huber G, Martin JR, Loffler J, Moreau JL (1993) Involvement of amyloid precursor protein in memory formation in the rat: an indirect antibody approach. Brain Res 603:348-352.

Jedlicka P, Owen M, Vnencak M, Tschape JA, Hick M, Muller UC, Deller T (2012) Functional consequences of the lack of amyloid precursor protein in the mouse dentate gyrus in vivo. Exp Brain Res 217:441-447.

Jo S et al. (2014) GABA from reactive astrocytes impairs memory in mouse models of Alzheimer's disease. Nat Med 20:886-896.

Johnson KA, Fox NC, Sperling RA, Klunk WE (2012) Brain imaging in Alzheimer disease. Cold Spring Harb Perspect Med 2:a006213.

Kabogo D, Rauw G, Amritraj A, Baker G, Kar S (2010) ss-amyloid-related peptides potentiate K+-evoked glutamate release from adult rat hippocampal slices. Neurobiol Aging 31:1164-1172.

Kamenetz F, Tomita T, Hsieh H, Seabrook G, Borchelt D, Iwatsubo T, Sisodia S, Malinow R (2003) APP processing and synaptic function. Neuron 37:925-937.

Kay KR, Smith C, Wright AK, Serrano-Pozo A, Pooler AM, Koffie R, Bastin ME, Bak TH, Abrahams S, Kopeikina KJ, McGuone D, Frosch MP, Gillingwater TH, Hyman BT, Spires-Jones TL (2013) Studying synapses in human brain with array tomography and electron microscopy. Nat Protoc 8:1366-1380.

Kirouac L, Rajic AJ, Cribbs DH, Padmanabhan J (2017) Activation of Ras-ERK Signaling and GSK-3 by Amyloid Precursor Protein and Amyloid Beta Facilitates Neurodegeneration in Alzheimer's Disease. eNeuro 4.

Klyubin I, Cullen WK, Hu NW, Rowan MJ (2012) Alzheimer's disease Abeta assemblies mediating rapid disruption of synaptic plasticity and memory. Mol Brain 5:25.

Klyubin I, Betts V, Welzel AT, Blennow K, Zetterberg H, Wallin A, Lemere CA, Cullen WK, Peng Y, Wisniewski T, Selkoe DJ, Anwyl R, Walsh DM, Rowan MJ (2008) Amyloid beta protein dimer-containing human CSF disrupts synaptic plasticity: prevention by systemic passive immunization. J Neurosci 28:4231-4237.

Koffie RM, Meyer-Luehmann M, Hashimoto T, Adams KW, Mielke ML, Garcia-Alloza M, Micheva KD, Smith SJ, Kim ML, Lee VM, Hyman BT, Spires-Jones TL (2009) Oligomeric amyloid beta associates with postsynaptic densities and correlates with excitatory synapse loss near senile plaques. Proc Natl Acad Sci U S A 106:4012-4017.

Koffie RM, Hashimoto T, Tai HC, Kay KR, Serrano-Pozo A, Joyner D, Hou S, Kopeikina KJ, Frosch MP, Lee VM, Holtzman DM, Hyman BT, Spires-Jones TL (2012) Apolipoprotein E4 effects in Alzheimer's disease are mediated by synaptotoxic oligomeric amyloid-beta. Brain 135:2155-2168.

Kohli BM, Pflieger D, Mueller LN, Carbonetti G, Aebersold R, Nitsch RM, Konietzko U (2012) Interactome of the amyloid precursor protein APP in brain reveals a protein network involved in synaptic vesicle turnover and a close association with Synaptotagmin-1. J Proteome Res 11:4075-4090.

Kurudenkandy FR, Zilberter M, Biverstal H, Presto J, Honcharenko D, Stromberg R, Johansson J, Winblad B, Fisahn A (2014) Amyloid-beta-induced action potential desynchronization and degradation of hippocampal gamma oscillations is prevented by interference with peptide conformation change and aggregation. J Neurosci 34:11416-11425.

Lacor PN, Buniel MC, Furlow PW, Clemente AS, Velasco PT, Wood M, Viola KL, Klein WL (2007) Abeta oligomer-induced aberrations in synapse composition, shape, and density provide a molecular basis for loss of connectivity in Alzheimer's disease. J Neurosci 27:796-807.

Lacor PN, Buniel MC, Chang L, Fernandez SJ, Gong Y, Viola KL, Lambert MP, Velasco PT, Bigio EH, Finch CE, Krafft GA, Klein WL (2004) Synaptic targeting by Alzheimer's-related amyloid beta oligomers. J Neurosci 24:10191-10200.

Lambert MP, Barlow AK, Chromy BA, Edwards C, Freed R, Liosatos M, Morgan TE, Rozovsky I, Trommer B, Viola KL, Wals P, Zhang C, Finch CE, Krafft GA, Klein WL (1998) Diffusible, nonfibrillar ligands derived from Abeta1-42 are potent central nervous system neurotoxins. Proc Natl Acad Sci U S A 95:6448-6453.

Lassek M, Weingarten J, Einsfelder U, Brendel P, Muller U, Volknandt W (2013) Amyloid precursor proteins are constituents of the presynaptic active zone. J Neurochem 127:48-56.

Lassek M, Weingarten J, Acker-Palmer A, Bajjalieh SM, Muller U, Volknandt W (2014) Amyloid precursor protein knockout diminishes synaptic vesicle proteins at the presynaptic active zone in mouse brain. Curr Alzheimer Res 11:971-980.

Lassek M, Weingarten J, Wegner M, Mueller BF, Rohmer M, Baeumlisberger D, Arrey TN, Hick M, Ackermann J, Acker-Palmer A, Koch I, Muller U, Karas M, Volknandt W (2016) APP Is a Context-Sensitive Regulator of the Hippocampal Presynaptic Active Zone. PLoS Comput Biol 12:e1004832.

Lauren J, Gimbel DA, Nygaard HB, Gilbert JW, Strittmatter SM (2009) Cellular prion protein mediates impairment of synaptic plasticity by amyloid-beta oligomers. Nature 457:1128-1132.

Lesne S, Koh MT, Kotilinek L, Kayed R, Glabe CG, Yang A, Gallagher M, Ashe KH (2006) A specific amyloid-beta protein assembly in the brain impairs memory. Nature 440:352-357.

Li S, Hong S, Shepardson NE, Walsh DM, Shankar GM, Selkoe D (2009) Soluble oligomers of amyloid Beta protein facilitate hippocampal long-term depression by disrupting neuronal glutamate uptake. Neuron 62:788-801.

Li S, Jin M, Koeglsperger T, Shepardson NE, Shankar GM, Selkoe DJ (2011) Soluble Abeta oligomers inhibit long-term potentiation through a mechanism involving excessive activation of extrasynaptic NR2B-containing NMDA receptors. J Neurosci 31:6627-6638.

Lillis KP, Wang Z, Mail M, Zhao GQ, Berdichevsky Y, Bacskai B, Staley KJ (2015) Evolution of Network Synchronization during Early Epileptogenesis Parallels Synaptic Circuit Alterations. J Neurosci 35:9920-9934.

Lorenzo A, Yuan M, Zhang Z, Paganetti PA, Sturchler-Pierrat C, Staufenbiel M, Mautino J, Vigo FS, Sommer B, Yankner BA (2000) Amyloid beta interacts with the amyloid precursor protein: a potential toxic mechanism in Alzheimer's disease. Nat Neurosci 3:460-464.

Mably AJ, Kanmert D, Mc Donald JM, Liu W, Caldarone BJ, Lemere CA, O'Nuallain B, Kosik KS, Walsh DM (2015) Tau immunization: a cautionary tale? Neurobiol Aging 36:1316-1332.

Mc Donald JM, O'Malley TT, Liu W, Mably AJ, Brinkmalm G, Portelius E, Wittbold WM, 3rd, Frosch MP, Walsh DM (2015) The aqueous phase of Alzheimer's disease brain contains assemblies built from approximately 4 and approximately 7 kDa Abeta species. Alzheimers Dement 11:1286-1305.

Melchor JP, Van Nostrand WE (2000) Fibrillar amyloid beta-protein mediates the pathologic accumulation of its secreted precursor in human cerebrovascular smooth muscle cells. J Biol Chem 275:9782-9791.

Melnikova T, Fromholt S, Kim H, Lee D, Xu G, Price A, Moore BD, Golde TE, Felsenstein KM, Savonenko A, Borchelt DR (2013) Reversible pathologic and cognitive phenotypes in an inducible model of Alzheimer-amyloidosis. J Neurosci 33:3765-3779.

Mileusnic R, Lancashire CL, Johnston AN, Rose SP (2000) APP is required during an early phase of memory formation. Eur J Neurosci 12:4487-4495.

Minkeviciene R, Rheims S, Dobszay MB, Zilberter M, Hartikainen J, Fulop L, Penke B, Zilberter Y, Harkany T, Pitkanen A, Tanila H (2009) Amyloid beta-induced neuronal hyperexcitability triggers progressive epilepsy. J Neurosci 29:3453-3462.

Mockett BG, Richter M, Abraham WC, Muller UC (2017) Therapeutic Potential of Secreted Amyloid Precursor Protein APPsalpha. Front Mol Neurosci 10:30.

Muller UC, Zheng H (2012) Physiological functions of APP family proteins. Cold Spring Harb Perspect Med 2:a006288.

Neve RL, McPhie DL (2007) Dysfunction of amyloid precursor protein signaling in neurons leads to DNA synthesis and apoptosis. Biochim Biophys Acta 1772:430-437.

Nimmrich V, Grimm C, Draguhn A, Barghorn S, Lehmann A, Schoemaker H, Hillen H, Gross G, Ebert U, Bruehl C (2008) Amyloid beta oligomers (A beta(1-42) globulomer) suppress spontaneous synaptic activity by inhibition of P/Q-type calcium currents. J Neurosci 28:788-797.

Ollion J, Cochennec J, Loll F, Escude C, Boudier T (2013) TANGO: a generic tool for high-throughput 3D image analysis for studying nuclear organization. Bioinformatics 29:1840-1841.

Palop JJ, Mucke L (2010) Amyloid-beta-induced neuronal dysfunction in Alzheimer's disease: from synapses toward neural networks. Nat Neurosci 13:812-818.

Palop JJ, Mucke L (2016) Network abnormalities and interneuron dysfunction in Alzheimer disease. Nat Rev Neurosci 17:777-792.

Parodi J, Sepulveda FJ, Roa J, Opazo C, Inestrosa NC, Aguayo LG (2010) Beta-amyloid causes depletion of synaptic vesicles leading to neurotransmission failure. J Biol Chem 285:2506-2514.

Pickett EK, Koffie RM, Wegmann S, Henstridge CM, Herrmann AG, Colom-Cadena M, Lleo A, Kay KR, Vaught M, Soberman R, Walsh DM, Hyman BT, Spires-Jones TL (2016) Non-Fibrillar Oligomeric Amyloid-beta within Synapses. J Alzheimers Dis 53:787-800.

Pliassova A, Lopes JP, Lemos C, Oliveira CR, Cunha RA, Agostinho P (2016) The Association of Amyloid-beta Protein Precursor With alpha- and beta-Secretases in Mouse Cerebral Cortex Synapses Is Altered in Early Alzheimer's Disease. Mol Neurobiol 53:5710-5721.

Portelius E, Olsson M, Brinkmalm G, Ruetschi U, Mattsson N, Andreasson U, Gobom J, Brinkmalm A, Holtta M, Blennow K, Zetterberg H (2013) Mass spectrometric characterization of amyloid-beta species in the 7PA2 cell model of Alzheimer's disease. J Alzheimers Dis 33:85-93.

Ring S, Weyer SW, Kilian SB, Waldron E, Pietrzik CU, Filippov MA, Herms J, Buchholz C, Eckman CB, Korte M, Wolfer DP, Muller UC (2007) The secreted beta-amyloid precursor protein ectodomain APPs alpha is sufficient to rescue the anatomical, behavioral, and electrophysiological abnormalities of APP-deficient mice. J Neurosci 27:7817-7826.

Ripoli C, Piacentini R, Riccardi E, Leone L, Li Puma DD, Bitan G, Grassi C (2013) Effects of different amyloid beta-protein analogues on synaptic function. Neurobiol Aging 34:1032-1044.

Russell CL, Semerdjieva S, Empson RM, Austen BM, Beesley PW, Alifragis P (2012) Amyloid-beta acts as a regulator of neurotransmitter release disrupting the interaction between synaptophysin and VAMP2. PLoS One 7:e43201.

Scheff SW, Price DA, Schmitt FA, Mufson EJ (2006) Hippocampal synaptic loss in early Alzheimer's disease and mild cognitive impairment. Neurobiol Aging 27:1372-1384.

Scheff SW, Price DA, Schmitt FA, DeKosky ST, Mufson EJ (2007) Synaptic alterations in CA1 in mild Alzheimer disease and mild cognitive impairment. Neurology 68:1501-1508.

Schindelin J, Arganda-Carreras I, Frise E, Kaynig V, Longair M, Pietzsch T, Preibisch S, Rueden C, Saalfeld S, Schmid B, Tinevez JY, White DJ, Hartenstein V, Eliceiri K, Tomancak P, Cardona A (2012) Fiji: an open-source platform for biological-image analysis. Nat Methods 9:676-682.

Schwenk J, Perez-Garci E, Schneider A, Kollewe A, Gauthier-Kemper A, Fritzius T, Raveh A, Dinamarca MC, Hanuschkin A, Bildl W, Klingauf J, Gassmann M, Schulte U, Bettler B, Fakler B (2016) Modular composition and dynamics of native GABAB receptors identified by high-resolution proteomics. Nat Neurosci 19:233-242.

Seabrook GR, Smith DW, Bowery BJ, Easter A, Reynolds T, Fitzjohn SM, Morton RA, Zheng H, Dawson GR, Sirinathsinghji DJ, Davies CH, Collingridge GL, Hill RG (1999) Mechanisms contributing to the deficits in hippocampal synaptic plasticity in mice lacking amyloid precursor protein. Neuropharmacology 38:349-359.

Shaked GM, Kummer MP, Lu DC, Galvan V, Bredesen DE, Koo EH (2006) Abeta induces cell death by direct interaction with its cognate extracellular domain on APP (APP 597-624). FASEB J 20:1254-1256.

Shankar GM, Welzel AT, McDonald JM, Selkoe DJ, Walsh DM (2011) Isolation of low-n amyloid beta-protein oligomers from cultured cells, CSF, and brain. Methods Mol Biol 670:33-44.

Shankar GM, Li S, Mehta TH, Garcia-Munoz A, Shepardson NE, Smith I, Brett FM, Farrell MA, Rowan MJ, Lemere CA, Regan CM, Walsh DM, Sabatini BL, Selkoe DJ (2008) Amyloid-beta protein dimers isolated directly from Alzheimer's brains impair synaptic plasticity and memory. Nat Med 14:837-842.

Soba P, Eggert S, Wagner K, Zentgraf H, Siehl K, Kreger S, Lower A, Langer A, Merdes G, Paro R, Masters CL, Muller U, Kins S, Beyreuther K (2005) Homo- and heterodimerization of APP family members promotes intercellular adhesion. EMBO J 24:3624-3634.

Sokolow S, Luu SH, Nandy K, Miller CA, Vinters HV, Poon WW, Gylys KH (2012) Preferential accumulation of amyloid-beta in presynaptic glutamatergic terminals (VGluT1 and VGluT2) in Alzheimer's disease cortex. Neurobiol Dis 45:381-387.

Sola Vigo F, Kedikian G, Heredia L, Heredia F, Anel AD, Rosa AL, Lorenzo A (2009) Amyloid-beta precursor protein mediates neuronal toxicity of amyloid beta through Go protein activation. Neurobiol Aging 30:1379-1392.

Steinbach JP, Muller U, Leist M, Li ZW, Nicotera P, Aguzzi A (1998) Hypersensitivity to seizures in beta-amyloid precursor protein deficient mice. Cell Death Differ 5:858-866.

Tamayev R, Matsuda S, Arancio O, D'Adamio L (2012) beta- but not gamma-secretase proteolysis of APP causes synaptic and memory deficits in a mouse model of dementia. EMBO Mol Med 4:171-179.

Tanzi RE (2012) The genetics of Alzheimer disease. Cold Spring Harb Perspect Med 2.

Van Nostrand WE, Melchor JP, Keane DM, Saporito-Irwin SM, Romanov G, Davis J, Xu F (2002) Localization of a fibrillar amyloid beta-protein binding domain on its precursor. J Biol Chem 277:36392-36398.

Vertkin I, Styr B, Slomowitz E, Ofir N, Shapira I, Berner D, Fedorova T, Laviv T, Barak-Broner N, Greitzer-Antes D, Gassmann M, Bettler B, Lotan I, Slutsky I (2015) GABAB receptor deficiency causes failure of neuronal homeostasis in hippocampal networks. Proc Natl Acad Sci U S A 112:E3291-3299.

Walsh DM, Teplow DB (2012) Alzheimer's disease and the amyloid beta-protein. Prog Mol Biol Transl Sci 107:101-124.

Walsh DM, Klyubin I, Fadeeva JV, Cullen WK, Anwyl R, Wolfe MS, Rowan MJ, Selkoe DJ (2002) Naturally secreted oligomers of amyloid beta protein potently inhibit hippocampal long-term potentiation in vivo. Nature 416:535-539.

Wang B, Wang Z, Sun L, Yang L, Li H, Cole AL, Rodriguez-Rivera J, Lu HC, Zheng H (2014) The amyloid precursor protein controls adult hippocampal neurogenesis through GABAergic interneurons. J Neurosci 34:13314-13325.

Wang HW, Pasternak JF, Kuo H, Ristic H, Lambert MP, Chromy B, Viola KL, Klein WL, Stine WB, Krafft GA, Trommer BL (2002) Soluble oligomers of beta amyloid (1-42) inhibit long-term potentiation but not long-term depression in rat dentate gyrus. Brain Res 924:133-140.

Wang ZM, Qi YJ, Wu PY, Zhu Y, Dong YL, Cheng ZX, Zhu YH, Dong Y, Ma L, Zheng P (2008) Neuroactive steroid pregnenolone sulphate inhibits long-term potentiation via activation of alpha2-adrenoreceptors at excitatory synapses in rat medial prefrontal cortex. Int J Neuropsychopharmacol 11:611-624.

Welzel AT, Maggio JE, Shankar GM, Walker DE, Ostaszewski BL, Li S, Klyubin I, Rowan MJ, Seubert P, Walsh DM, Selkoe DJ (2014) Secreted amyloid beta-proteins in a cell culture model include N-terminally extended peptides that impair synaptic plasticity. Biochemistry 53:3908-3921.

White AR, Zheng H, Galatis D, Maher F, Hesse L, Multhaup G, Beyreuther K, Masters CL, Cappai R (1998) Survival of cultured neurons from amyloid precursor protein knock-out mice against Alzheimer's amyloid-beta toxicity and oxidative stress. J Neurosci 18:6207-6217.

Wilhelm BG, Mandad S, Truckenbrodt S, Krohnert K, Schafer C, Rammner B, Koo SJ, Classen GA, Krauss M, Haucke V, Urlaub H, Rizzoli SO (2014) Composition of isolated synaptic boutons reveals the amounts of vesicle trafficking proteins. Science 344:1023-1028.

Willem M et al. (2015) eta-Secretase processing of APP inhibits neuronal activity in the hippocampus. Nature 526:443-447.

Yang L, Wang Z, Wang B, Justice NJ, Zheng H (2009) Amyloid precursor protein regulates Cav1.2 L-type calcium channel levels and function to influence GABAergic short-term plasticity. J Neurosci 29:15660-15668.

Yang T, Li S, Xu H, Walsh DM, Selkoe DJ (2017) Large Soluble Oligomers of Amyloid beta-Protein from Alzheimer Brain Are Far Less Neuroactive Than the Smaller Oligomers to Which They Dissociate. J Neurosci 37:152-163.

Yang T, O'Malley TT, Kanmert D, Jerecic J, Zieske LR, Zetterberg H, Hyman BT, Walsh DM, Selkoe DJ (2015) A highly sensitive novel immunoassay specifically detects low levels of soluble Abeta oligomers in human cerebrospinal fluid. Alzheimers Res Ther 7:14.

Yankner BA, Lu T (2009) Amyloid beta-protein toxicity and the pathogenesis of Alzheimer disease. J Biol Chem 284:4755-4759.

Zhang D, Mably AJ, Walsh DM, Rowan MJ (2016) Peripheral Interventions Enhancing Brain Glutamate Homeostasis Relieve Amyloid beta- and TNFalpha- Mediated Synaptic Plasticity Disruption in the Rat Hippocampus. Cereb Cortex.

Zheng H, Jiang M, Trumbauer ME, Sirinathsinghji DJ, Hopkins R, Smith DW, Heavens RP, Dawson GR, Boyce S, Conner MW, Stevens KA, Slunt HH, Sisoda SS, Chen HY, Van der Ploeg LH (1995) beta-Amyloid precursor protein-deficient mice show reactive gliosis and decreased locomotor activity. Cell 81:525-531.

Zucker RS, Regehr WG (2002) Short-term synaptic plasticity. Annu Rev Physiol 64:355-405.

Table 1. Primary and secondary antibodies.

Antibody	Type	Antigen/epitope	Dilution for IP	Conc. For WB	Conc. For ELISA	Dilution for AT	Source/Reference
3D6	Monoclonal	Aβ1–5	–	-	1 µg/ml	–	Elan/(Johnson-Wood et al., 1997)
6E10	Monoclonal	Aβ3-8	-	1 µg/ml	-	-	Biolegend/(Kim et al. 1988)
266	Monoclonal	Aβ16-23	–	-	3 µg/ml	–	Elan/(Seubert et al., 1992)
2G3	Monoclonal	Aβ terminating at Val40	–	1 µg/ml	–	–	Elan/(Johnson-Wood et al., 1997)
21F12	Monoclonal	Aβ terminating at Ile42	–	1 µg/ml	1 µg/ml	–	Elan/(Johnson-Wood et al., 1997)
1C22	Monoclonal	Aβ aggregates	–	–	3 µg/ml	1:50	Walsh lab/(Mably et al., 2015)
AW7	Polyclonal	Pan anti-Aβ	1:80	–	–	–	Walsh lab/(Mc Donald et al., 2012)
22C11	Monoclonal	APP66-81	–	1 µg/ml	–	1:50	Millipore/(Austin et al., 2009)
AB1543P	Polyclonal	Rabbit anti-synapsin-1	–	–	–	1:100	Millipore/(Kay et al., 2013)
3450P	Polyclonal	Rabbit anti-PSD95	–	–	–	1:50	Cell Signaling/(Kay et al., 2013)
A21202	Polyclonal	Donkey anti-mouse 488	–	–	–	1:50	Invitrogen
A21207	Polyclonal	Donkey anti-rabbit 594	–	–	–	1:50	Invitrogen
T6074	Monoclonal	Anti-α-Tubulin	–	1 µg/ml	–	–	Sigma

Figure 1: Processing of array tomography images.

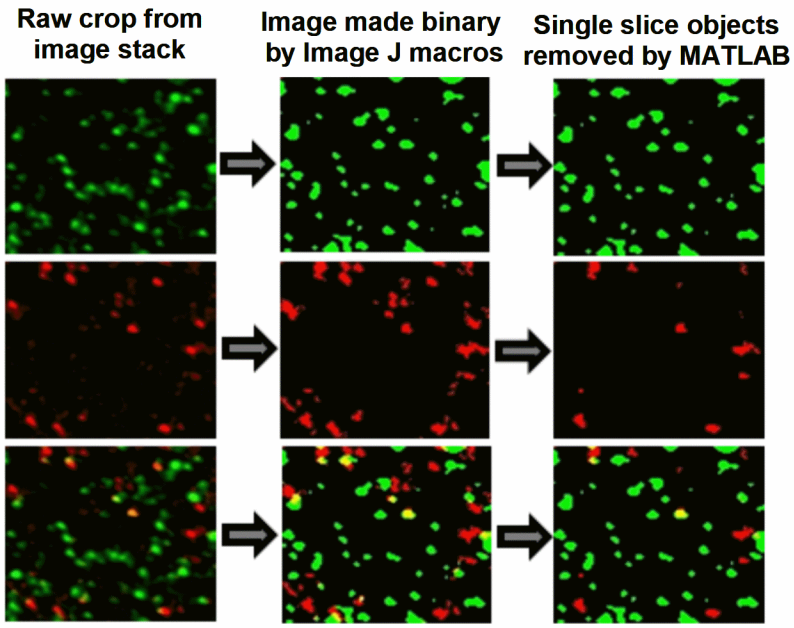

Figure 2: The water-soluble extract of AD brain, but not normal control, contains both Aβ monomers and oligomers and perturbs long-term synaptic plasticity.

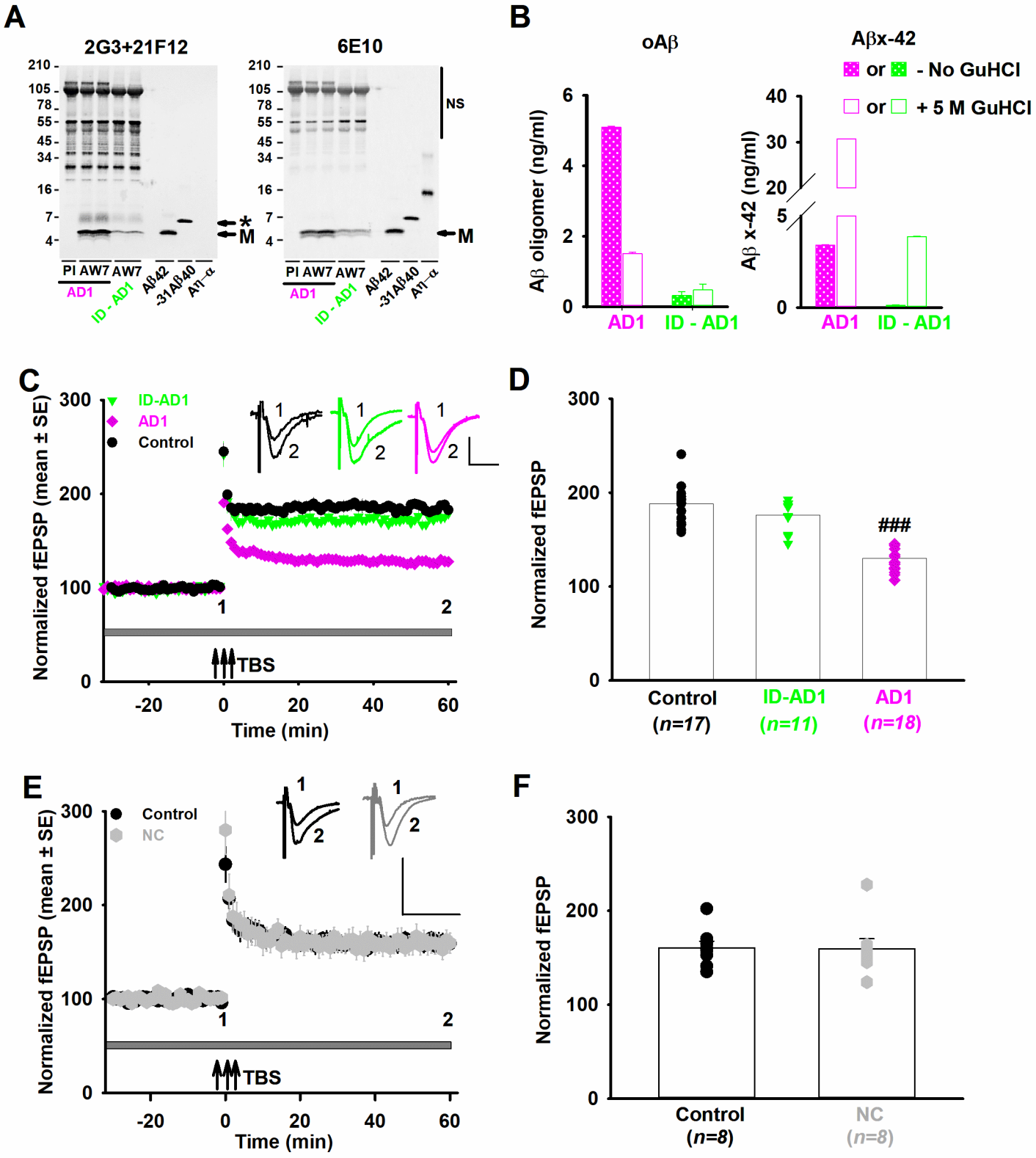

Figure 3: The Aβ-containing water-soluble extract of AD1 perturbs short-term facilitation.

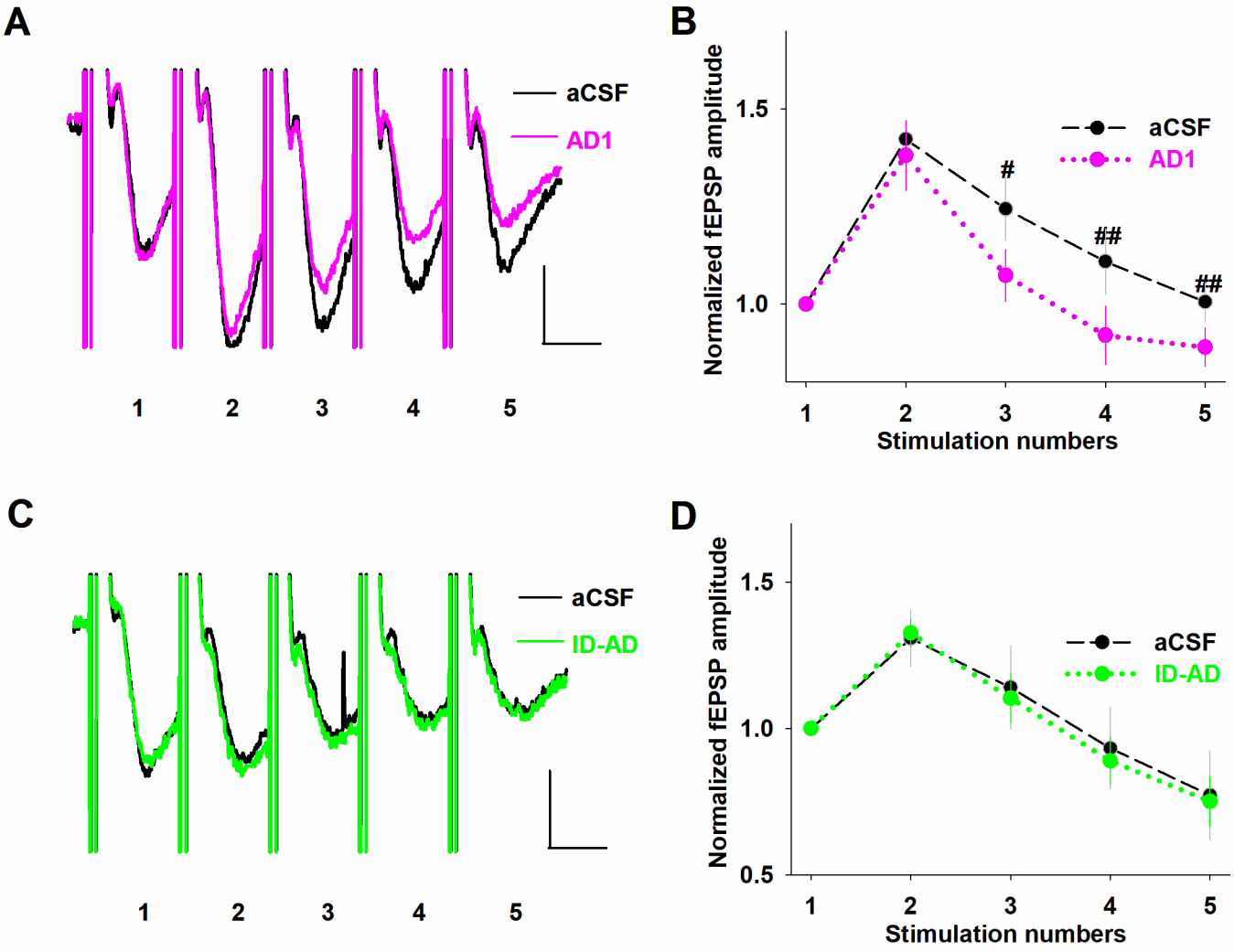

Figure 4: AD brain-derived Aβ affects both excitatory and inhibitory synaptic inputs, causing disruption of the excitatory/inhibitory ratio at individual CA1 neurons.

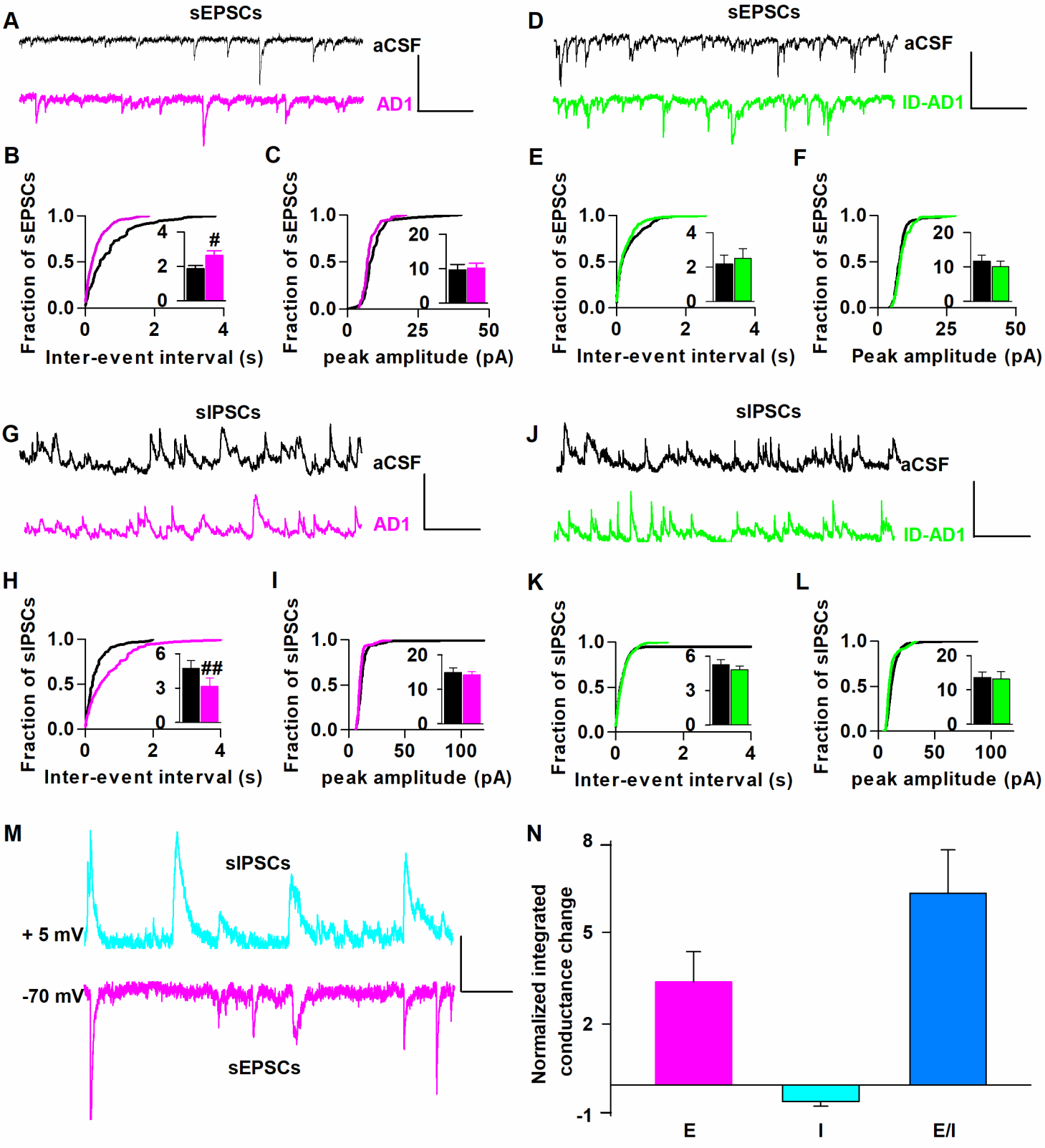

Figure 5: Expression of APP is required for the plasticity-disrupting activity of Aβ-containing AD brain extract.

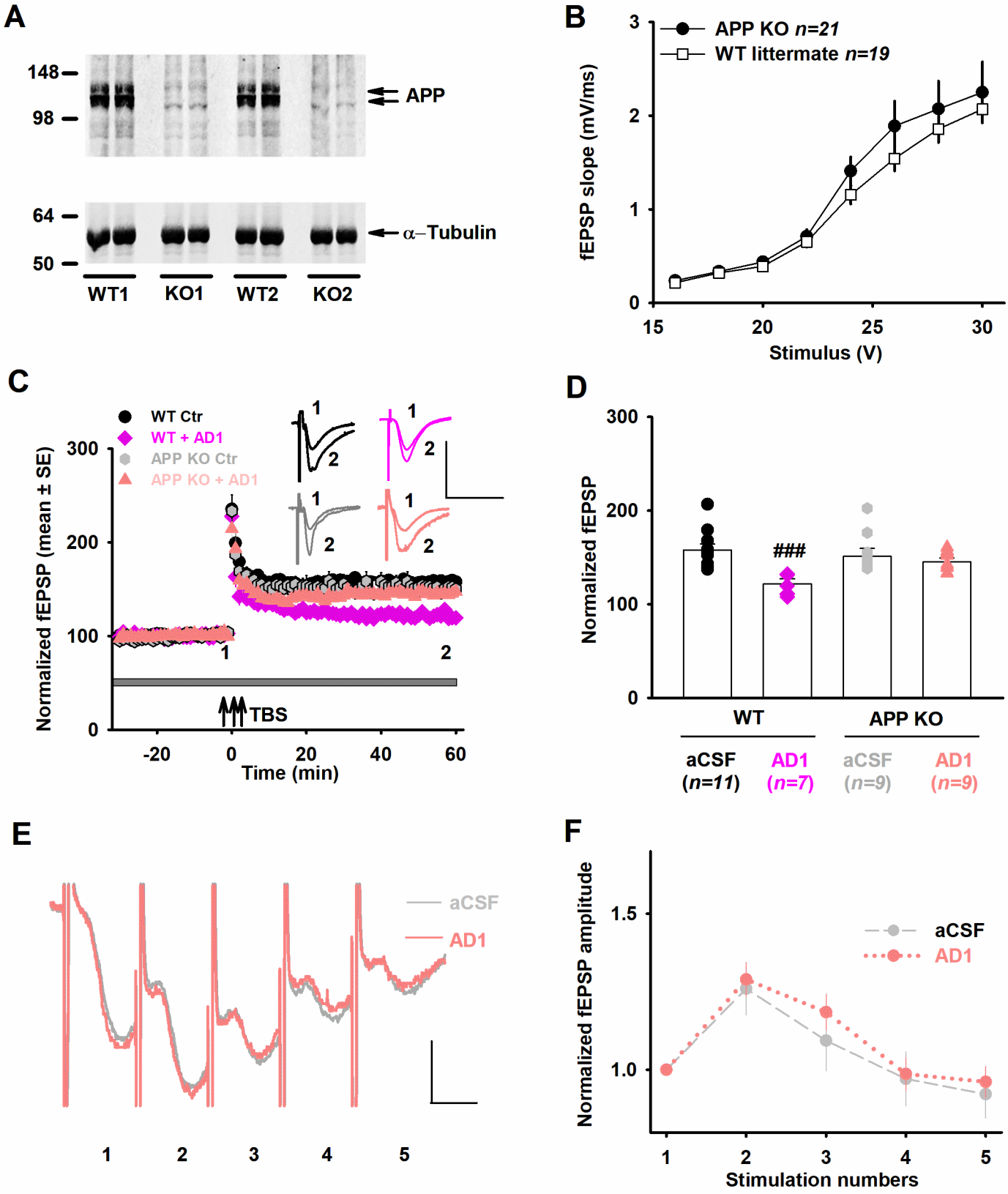

Figure 6: Characterization of the aqueous extract from AD2 brain, synthetic Aβ oligomers and a second APP KO mouse line.

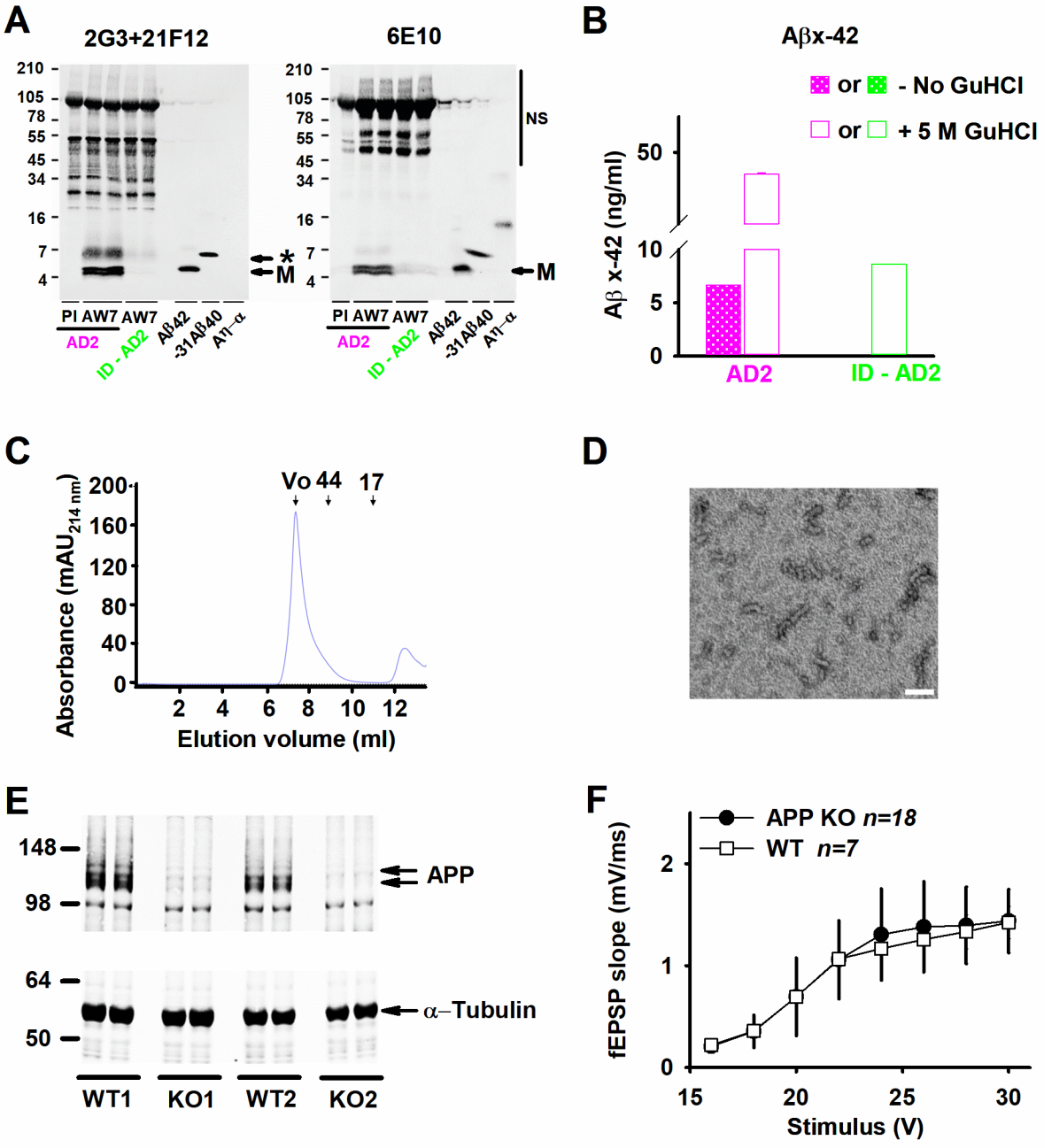

Figure 7: A second APP KO mouse line confirms that APP is required for the synaptic-disrupting activity of both AD brain and sythetic Aβ oligomers.

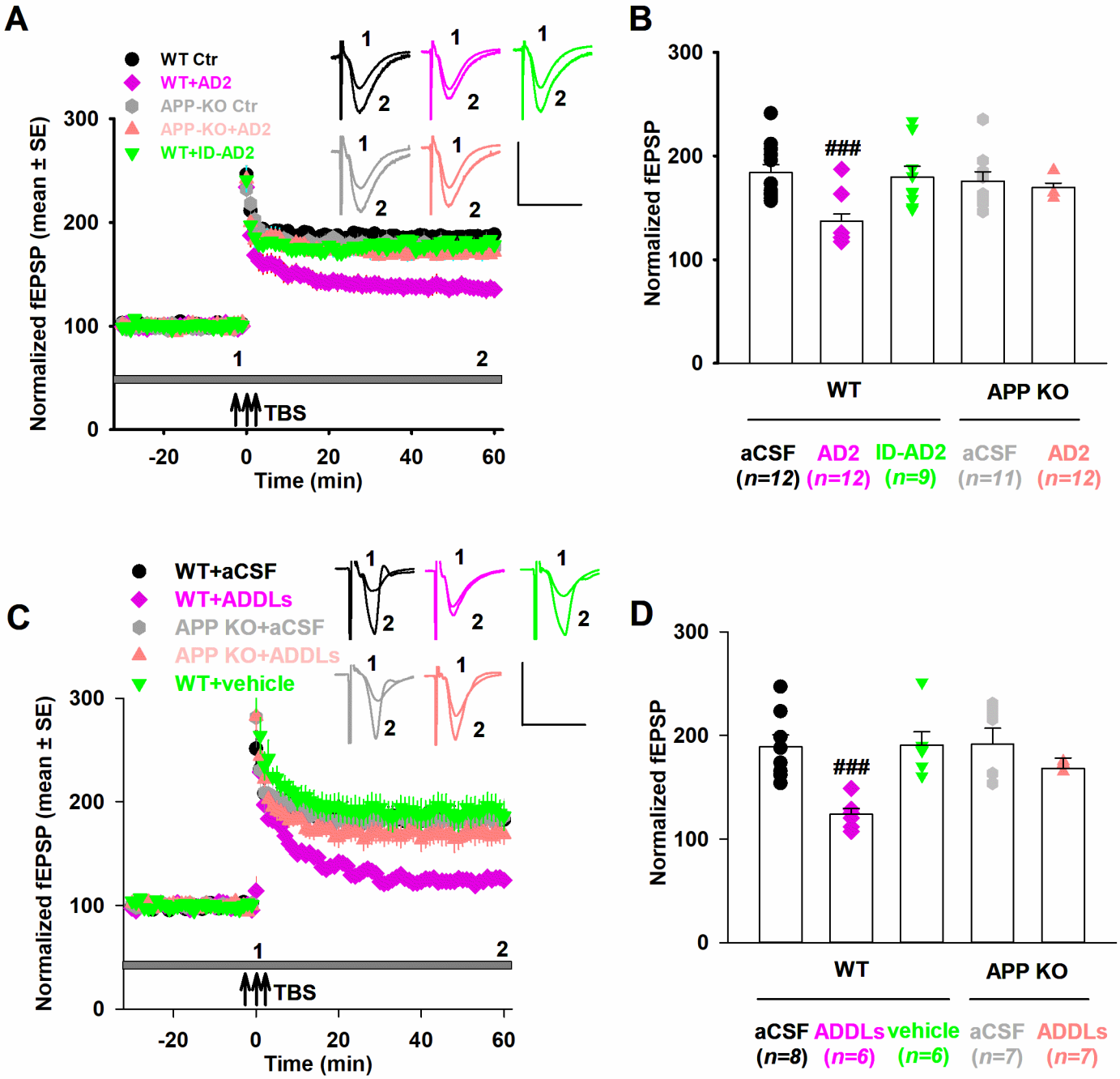

Figure 8: APP knock out occludes the effects of Aβ-containing AD brain extract on both excitatory and inhibitory postsynaptic currents and rescues the disruption of E/I balance.

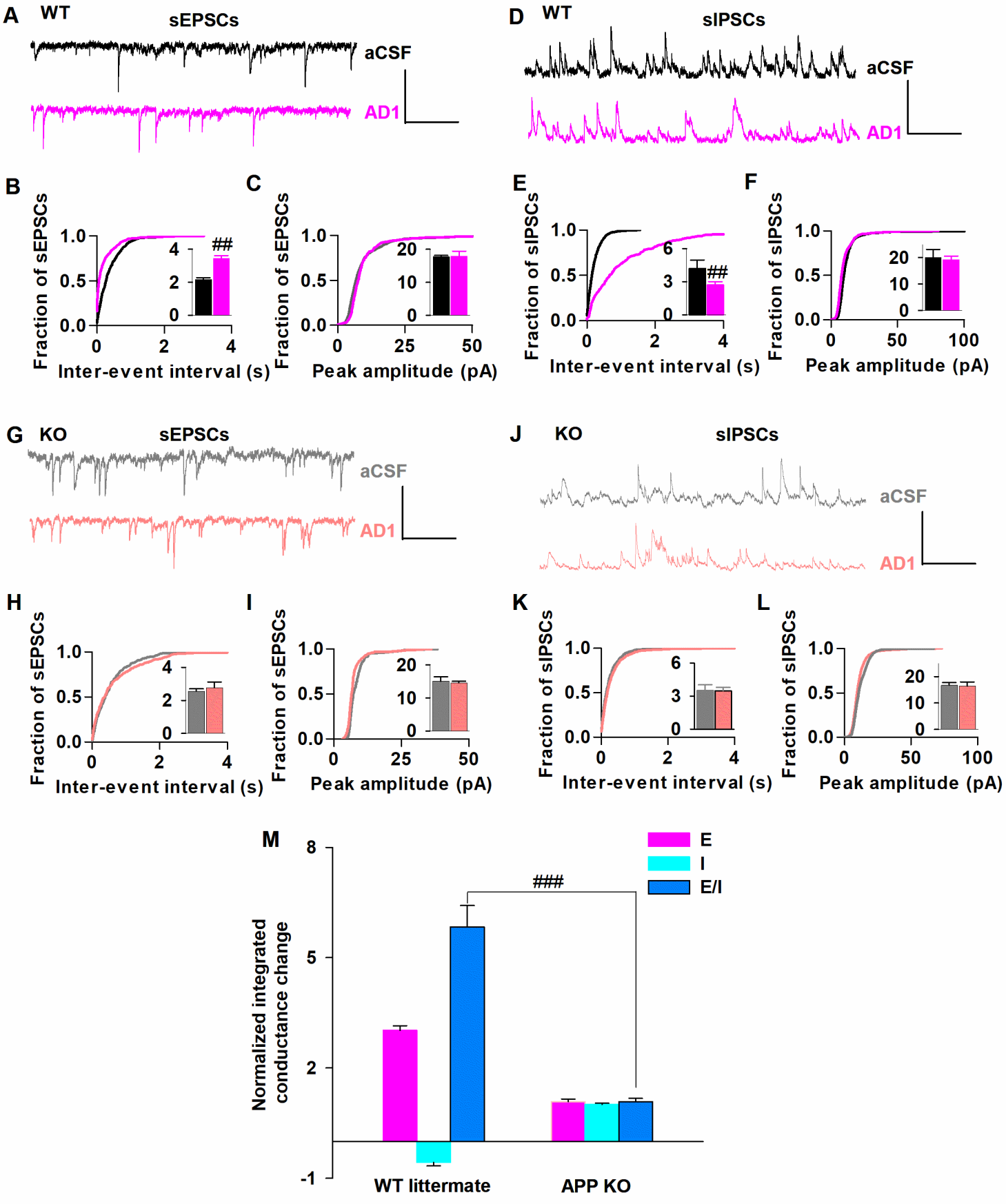

Figure 9: Aβ binding to synaptic terminals requires experssion of APP.

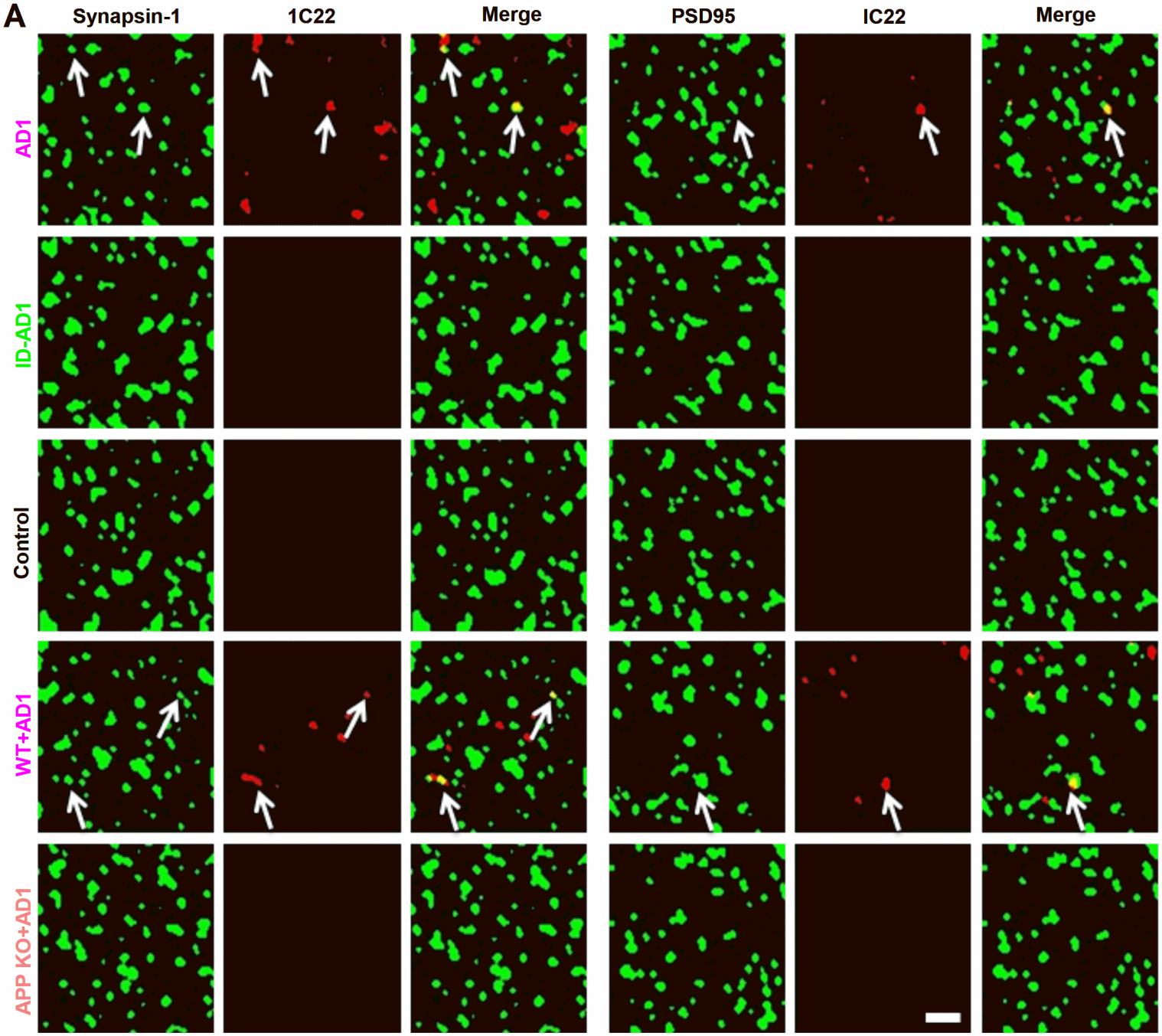

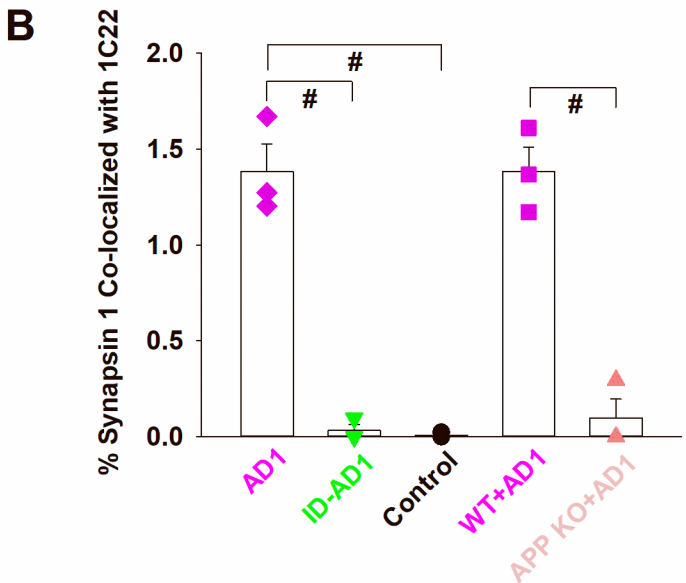

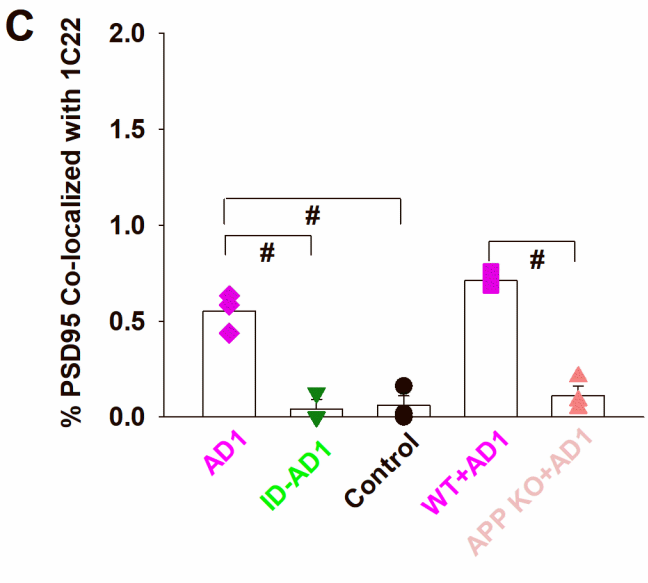

Figure 10: APP expressing, but not APP lacking brain slices bind synaptotoxic Aβ.

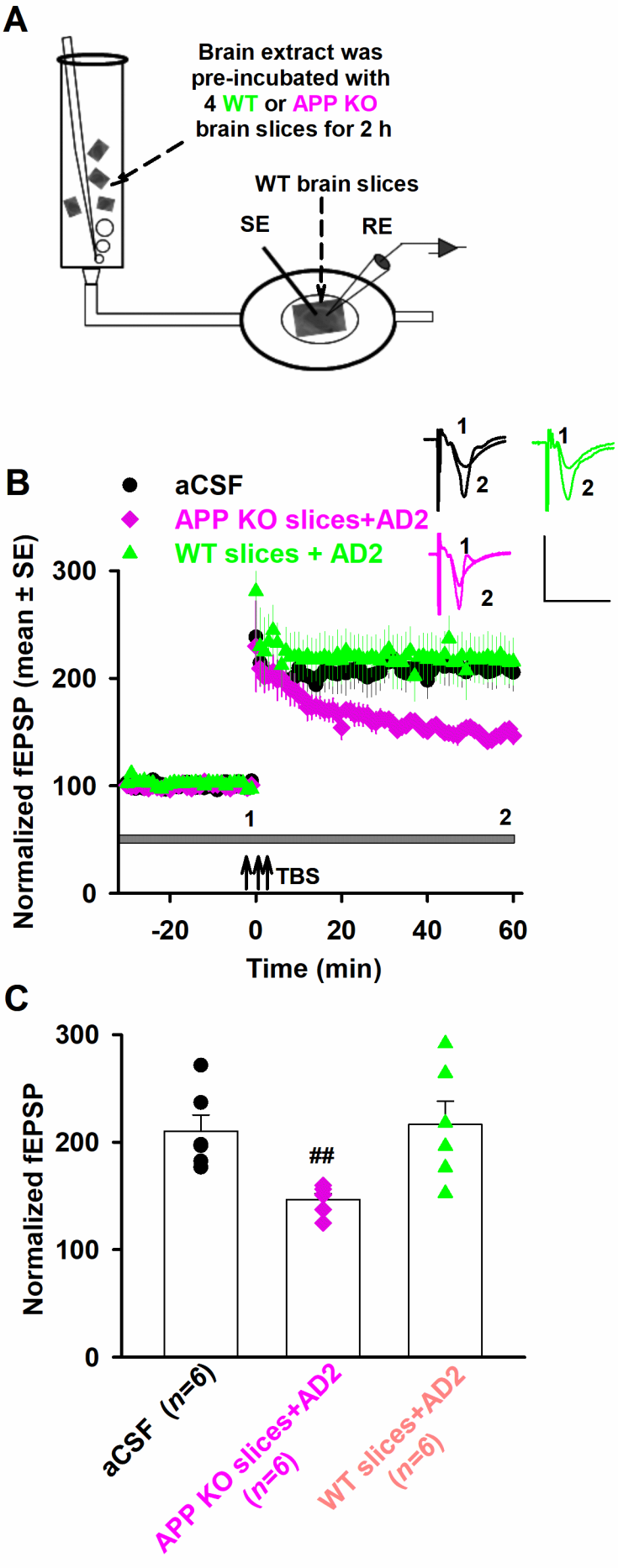

Figure 11: The level of APP expression influences the plasticity-disrupting activity of Aβ-containing AD brain extract.